Moteki
Progress in Earth and Planetary Science 2023, **10**(1):12
https://doi.org/10.1186/s40645-023-00544-4

Progress in Earth and Planetary Science

REVIEW

Open Access

Climate-relevant properties of black carbon aerosols revealed by in situ measurements: a review

Nobuhiro Moteki[1*]

Abstract

Light-absorbing aerosols affect atmospheric radiation, dynamics, and precipitations through shortwave absorption in the atmosphere and snowpack. Black carbon (BC) is considered the most significant contributor to global shortwave absorption among all the known light-absorbing aerosol components. In analyses and predictions of BC's lifecycle and climate effects, multiscale field observations are needed to test the fundamental assumptions in the climate model. In situ measurements, the focus of this review, fill the gap of observational information accessible from remote sensing and laboratory analyses. This article reviews historical backgrounds, recent advances in in situ measurements of BC, and the resulting observational findings used to update the assumptions in climate models and remote sensing. Finally, we raise open problems that demand a rethinking and future investigation.

Keywords Atmospheric chemistry, Atmospheric radiation, Climate, Aerosol, Light-absorbing aerosols, Black carbon

1 Introduction

1.1 Light-absorbing aerosols

Light-absorbing aerosol components exert complex perturbations to the climate system through their shortwave absorption in the atmosphere and snowpack (Stier et al. 2007; Samset et al. 2018). The atmospheric heating by aerosol's shortwave absorption alters the circulation and precipitation from regional-to-global scales (Lau et al. 2006; Samset et al. 2022). Known significant contributors to aerosol's shortwave absorption are light-absorbing constituents of carbonaceous compounds (i.e., black carbon, brown carbon) and iron oxides (i.e., goethite, hematite, magnetite) from both anthropogenic and non-anthropogenic origins (e.g., Moteki et al. 2017).

Carbonaceous aerosol emitted as a byproduct of the combustions of fossil fuels, biofuels, and biomass is a mixture of a large variety of organic molecules and partly graphitized solid carbon (Lighty et al. 2000; Simoneit 2000). In addition, other organic molecules and polymers as secondary constituents of carbonaceous aerosol are produced in the atmosphere through gas-phase photochemical reactions and aqueous reactions in cloud droplets (Kalberer et al. 2004; Kanakidou et al. 2005; Ervens et al. 2011; Shrivastava et al. 2017). Carbonaceous aerosol materials can be categorized on the continuous spectrum of the imaginary part of the refractive index (Andreae and Gelencsér 2006; Corbin et al. 2019). One extreme of the spectrum is the group of non-refractory organic molecules with negligible imaginary refractive index, which is referred to as organic carbon (OC). Another spectrum extreme is the group of partly graphitized solid-state refractory material with a high imaginary refractive index, black carbon (BC) (Bond et al. 2013). The middle of the spectrum is a group of yellowish-to-brownish organic compounds with a moderate imaginary refractive index, commonly referred to as brown carbon (BrC) (Laskin et al. 2015). The BrC can also secondarily form through photochemical reactions in the atmosphere

*Correspondence:
Nobuhiro Moteki
moteki@eps.s.u-tokyo.ac.jp
[1] Department of Earth and Planetary Science, Graduate School of Science, The University of Tokyo, 7-3-1 Hongo, Bunkyo-Ku, Tokyo 113-0033, Japan

from primary and secondary OC materials (Updyke et al. 2012). The imaginary refractive index of BrC material can rapidly change as the BrC particles photochemically age in the atmosphere (Zhao et al. 2015). By contrast, BC is chemically inert in the atmosphere and even persistent after deposition on timescales from centuries to millennia (Coppola et al. 2022).

In this review, the author focused only on BC among all the light-absorbing aerosol components to elaborate on the recent advances in the in situ BC measurements and their contributions to the fundamental understanding of aerosol processes and the developments of the aerosol-climate model.

1.2 Black carbon

Owing to its high imaginary refractive index and relatively long atmospheric lifetime, BC is the largest contributor to global shortwave absorption in the present atmosphere among all the light-absorbing aerosol compounds (Samset et al. 2018; Sand et al. 2021). Atmospheric heating by BC reduces the global mean precipitation by compensating for the latent-heat transport from the surface to the atmosphere (Pendergrass and Hartmann 2012). BC deposited on snow-covered surfaces contributes to albedo reduction and accelerates the snowmelt (Flanner et al. 2007).

The morphology of each BC particle is known to be an aggregate of nanospheres. The diameter of each primary nanosphere (monomer) is typically 10–100 nm (Buseck et al. 2014). Each monomer consists of an onion-shell-like arrangement of graphene nanolayers (Buseck et al. 2014). The refractive index of each carbon monomer depends on the electronic structure of the carbon material, which is related to the degree of graphitization (Stagg and Charalampopoulos 1993; Bond and Bergstrom 2006). As the degree of graphitization of BC particles depends on the flame environment (Apicella et al. 2018), the refractive index of atmospheric BC could be variable depending on emission sources. The optical properties, such as the mass absorption cross section (MAC m^2/g), of each BC particle depend on the refractive index of consisting monomers, morphological parameters of aggregate, and aggregate's volume-equivalent size relative to the wavelength (Zheng and Wu 2021).

Each BC particle emitted from the combusting flame to the atmosphere rapidly undergoes internal mixing with other aerosol components (e.g., organic matter, sulfate, nitrate) through the condensation and coagulation process. Low-efficiency combustions such as wildfire produce high-concentration condensable organic molecules and carbonaceous aerosols with a high OC-to-BC ratio, resulting in instantaneous internal mixing of BC and OC within the dense smoke (Schwarz et al. 2008b). By contrast, relatively high-efficiency combustions such as vehicle engines produce carbonaceous aerosols with a much lower OC-to-BC ratio, resulting in the release of uncoated pure BC particles into the atmosphere (Schwarz et al. 2008b). Such BC particles undergo internal mixing with secondary aerosols (e.g., organics, sulfate) formed through the photochemical production of condensable gases from precursors (i.e., volatile organic compounds, sulfur dioxide, ammonia, etc.) (Shiraiwa et al. 2007; Riemer et al. 2010). Two dominant aerosol components mixed with BC are considered to be sulfate and organics because of the pervasiveness of these compounds in the atmosphere (Murphy et al. 1998; Thompson et al. 2022).

The BC-containing particles consisting of BC and non-BC materials are very different in climate-relevant properties from pure BC particles. Firstly, BC-containing particles consisting of BC core and non-absorbing coating materials have larger MAC per unit BC mass than pure BC particles due to enhancement of the electric field incident onto the BC core through "lensing effects" by the coating materials (Fuller et al. 1999). The MAC enhancement of ambient BC by coating may be up to ~ 60% depending on sources and aging (Liu et al. 2017). Secondly, BC-containing particles would be able to be cloud condensation nuclei (CCN) under modest supersaturations (~ 0.1%) in environmental clouds, whereas the pure BC particles are CCN inactive for their hydrophobic surface (Dusek et al. 2006; Kuwata et al. 2009). The coating materials on the BC core tend to become more hygroscopic with the aging of the plume (Ohata et al. 2016; Perring et al. 2017). The coating strongly affects the critical supersaturation of BC-containing particles in less-aged urban plumes (Zaveri et al. 2010). The thickness and hygroscopicity of the coating are, therefore, critical factors controlling the efficiency of vertical transport of BC through moist convection at the proximity of urban emission sources (Moteki et al. 2019).

In this review, we provide the historical backgrounds and recent advances of the in situ techniques for identifying and quantifying the BC and BC-containing particles after the mid-2000s. We clarify the unique roles of in situ BC measurements in recent advances in physical science basis on evaluating the effects of BC and other aerosols on climate (Fig. 1). This review on BC is intentionally focused on the research areas the author (N. Moteki) has made some original contributions, avoiding the areas already reviewed by previous studies (e.g., Bond and Bergstrom 2006; Ramanathan and Carmichael 2008; Moosmüller et al. 2009; Bond et al. 2013; Petzold et al. 2013; Kang et al. 2020; Liu et al. 2020a, b; Coppola et al. 2022).

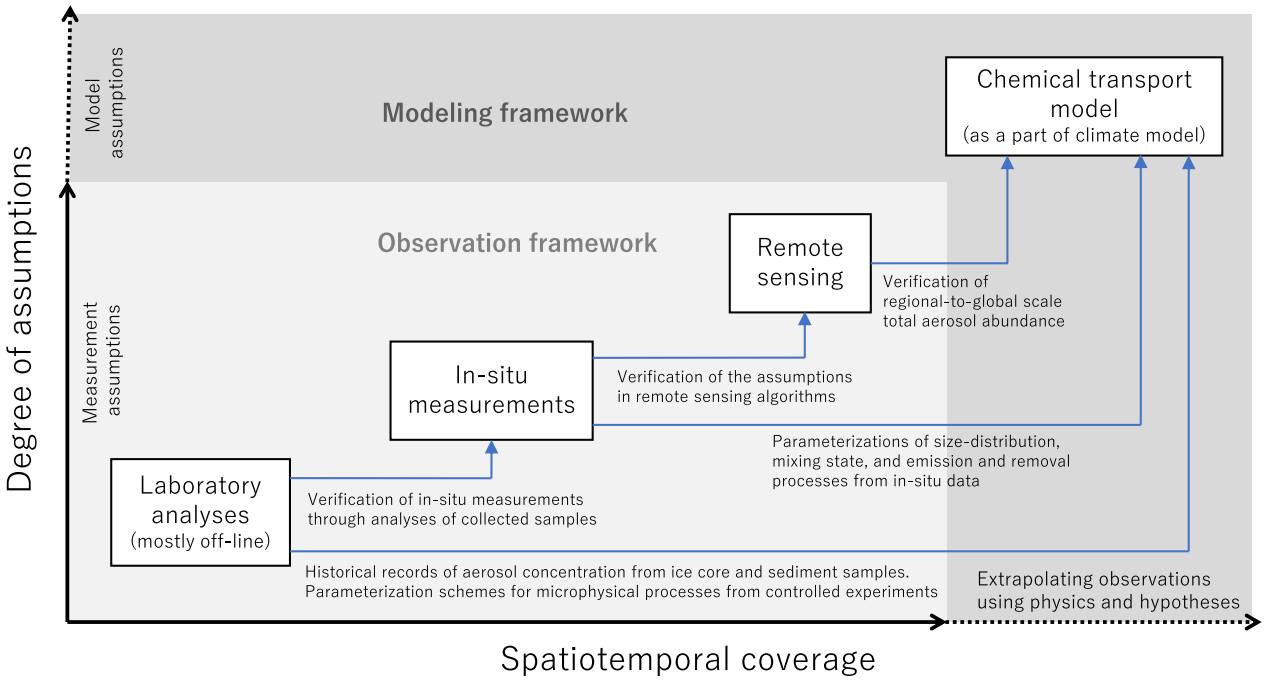

Fig. 1 Roles and relationships of the four different approaches in aerosol-climate research. Laboratory analyses of collected samples, in situ measurements, and remote sensing provide complementary observational information needed for reducing assumptions in the atmospheric chemical transport model (sub-module of the climate model)

2 Measurement techniques

2.1 Backgrounds

BC is a ubiquitous aerosol component from the troposphere to the stratosphere, but its abundance is only a tiny fraction (< 2%) of total submicron aerosols mass in the global atmosphere, most of which is contributed by sulfate and organics (Gao et al. 2022). The minority of BC in the total aerosol carbon with various physicochemical properties makes the robust thermochemical identification of BC difficult (Cavalli et al. 2010; Karanasiou et al. 2015). Bulk optical methods for quantifying BC according to the absorption spectrum of a population of aerosol particles require the assumptions of the spectral refractive index of every potential contributor to the measured light absorption (Yang et al. 2009; Schuster et al. 2016). In addition to the uncertainties of the spectral refractive index, the change of light absorption efficiency of each absorbing component with particle's size, morphology, and mixing state with non-absorbing compounds makes the bulk optical methods more susceptible to bias (Bond et al. 1999; Nakayama et al. 2010; Moteki et al. 2010a).

An observable particle-size measure of each BC aggregate depends on the measurement principle and procedure due to the non-spherical particle shape and internal mixing with other components (Kasper 1982; McMurry et al. 2002; Slowik et al. 2004; Kazemimanesh et al. 2022). BC aggregates change their original lacy shape to be more compact in the atmosphere as they experience collapsing through their aging and cloud processing (Bhandari et al. 2019). For these reasons, it has been difficult to quantify the size-resolved BC concentration with a size-sorting aerosol sampling followed by bulk BC analyses.

The single-particle laser-induced incandescence (LII) using an intracavity laser beam introduced around the mid-2000s (Stephens et al. 2003), a commercial version is known as single-particle soot photometer (SP2; Droplet Measurement Technologies Inc., Boulder, CO.), has extended our capability of identifying and quantifying atmospheric BC and BC-containing particles largely overcoming the difficulties mentioned above. The in situ data obtained by the SP2 instruments are routinely used in the aerosol-climate research community for investigating aerosol processes and testing and prescribing assumptions in other BC monitoring methods, aerosol remote sensing algorithms, and aerosol-climate models. We review the development history, principle, and known limitations of the single-particle LII in Sect. 2.2. We would use the word single-particle LII instead of SP2 as we focus here on the physical principle, independent of the supplier's actual implementation of the hardware and software.

Section 2.3 reviews complex amplitude sensing (CAS) (Moteki 2021), a generic method for single-particle optical characterization of liquid-borne particles, which is

also useful as a new approach for in situ BC measurements and explorations of BC refractive index.

2.2 Laser-induced incandescence

The laser-induced incandescence (LII) using pulsed lasers has long been used in combustion sciences for the noninvasive characterization of concentrations and microphysical properties of soot particles in flame (Vander Wal and Weiland 1994; Schulz et al. 2006; Michelsen et al. 2015). In the pulse LII approach, each high-energy pulse of a laser beam emitted from the light source (e.g., Nd:YAG laser) is expanded to irradiate a flaming volume that contains a population of soot particles. Then, the thermal radiation at visible-to-near-infrared wavelengths, also called incandescence, emitted from soot particles heated up to their vaporization point ~ 4200 K, is detected at several wavelength bands by photodetectors or image sensors. The simultaneous LII measurement at several (at least two) wavelength bands is needed for estimating the soot temperature from the spectral dependence of emitted thermal radiation. LII signal intensity at each wavelength band is proportional to the soot volume concentration within the sensing region. Imaging LII intensity distributions resolves the soot-forming regions and soot population growth within the flame (Ni et al. 1995). The rate of cooling of soot particles after the excitation pulse inferred from a fast time-resolved measurement of LII signals is used to estimate the mean monomer size of soot aggregates (Vander Wal et al. 1999; Axelsson et al. 2000). The pulse energy density for LII excitation within the sensing volume is determined between the lower limit that is needed to heat soot particles to vaporization point and the upper limit at which vaporization loss of soot during the pulse excitation starts to be apparent (Vander Wal and Jensen 1998). The laser wavelength for LII excitation should be selected to reduce the interferences from fluorescence emission of clusters of carbon atoms (Goulay et al. 2009). The longer excitation wavelengths are preferable to suppress fluorescence at the LII monitoring visible wavelengths, whereas the particle's heating efficiency is higher in shorter excitation wavelengths (Schulz et al. 2006). The near-infrared 1064 nm wavelength of Nd:YAG laser or its second harmonic 532 nm was primarily employed for LII excitation in practice (Michelsen et al. 2015).

Although the pulse LII approach is used for monitoring the volume concentration of BC particles in engine exhaust gases (Snelling et al. 1999), it is not practical for field observations due to the very low and highly variable BC concentrations in the atmosphere. Pulse-hit probability can be increased if the excitation pulse is triggered by the particle's scattering signal from another continuous wave (CW)-operating laser beam just upstream of the LII excitation region, as has been done in the single-particle laser mass spectrometers (Murphy 2007). Even so, BC detection frequency in ambient air samples will remain too low to obtain size-resolved statistics in real-time as the fraction of aerosol particles containing BC aggregate will be one-to-several orders of magnitude lower than BC-free particles (Matsui et al. 2011).

The particle detection frequency drawback of pulse LII for atmospheric applications has been concisely solved by the single-particle LII technique using an intracavity CW-laser beam (Stephens et al. 2003). The single-particle LII uses the CW-laser beam building up inside a solid-state laser cavity to excite the LII signal from every BC (and other metallic) particle in the sample gas jet focused into the intracavity beam. The original single-particle LII instrument by Stephens et al. (2003) employed the 1064 nm Nd:YAG laser cavity pumped by an 808 nm fiber-coupled diode laser ($< \sim 4$W). This diode-pumped Nd:YAG 1064 nm laser system has been employed by most of the single-particle LII instruments developed so far for its practical energy efficiency, stability, and cost advantages. The original instrument by Stephens et al. (2003) integrated four independent light-collection optics with different optical filters to be able to simultaneously monitor four different signals from each particle during its transition across the intracavity beam: three of which were used for LII signals at various wavelength bands, one of which was used for scattering signal at 1064 wavelength. The waveform of the scattering signal was initially used as an indicator of the particle's vaporization in the laser beam. An appreciable shrink of an incandescing particle in the laser beam is experimental evidence that the particle's temperature has reached the material-specific vaporization point at the peak of LII signals. The signal intensity ratios between the three LII channels were used for identifying incandescing material according to the difference in vaporization temperature. Although Stephens et al. (2003) demonstrated single-particle LII's capability to identify individual flame soot, graphite, and several metallic particles, they did not investigate the possibility of quantifying the climate-relevant properties of single BC particles (e.g., size, mixing state).

Baumgardner et al. (2004) reported the first application of a single-particle LII instrument (single-particle soot photometer: SP2 commercialized by Droplet Measurement Technologies) to field observations. Determining single-particle BC mass from the LII signal in field observations requires a laboratory calibration of their empirical relationship using an appropriate standard BC sample. Baumgardner et al. (2004) used a spherical glassy carbon powder to sort particle mass using a conventional electrical mobility particle-size classifier (Knutson and Whitby 1975). The potential artifacts of using the spherical glassy

carbon as an LII calibration standard material for quantifying non-spherical BC aggregates were not evaluated then.

Schwarz et al. (2006) and Slowik et al. (2007) employed flame-generated soot as more similar materials with ambient BC aggregates for calibrating the LII-to-mass relationship within 2–30 fg mass range (130–320 nm volume-equivalent diameter d_v, assuming 1.8 g cm^{-3} density). In the calibration, they indirectly estimated the mass of flame-generated soot particles sorted at a particular mobility diameter by scanning their distribution in vacuum aerodynamic diameter, as a direct method for sorting the mass of non-spherical aerosol particles had not yet been available. Schwarz et al. (2006) observed that the LII signal amplitude was linearly proportional to the mass of flame-generated soot at 2–30 fg and that the linear relationship (e.g., slope) was unchanged with the fractal dimension of soot aggregates. They employed the linear LII-to-mass relationship for ambient BC measurements, extrapolating the calibration line at mass $\leq$ 30 fg to larger particles up to ~ 800 fg (d_v ~ 950 nm). Although the accuracy of this extrapolation had not been thoroughly evaluated then, Schwarz et al. (2006) are regarded as a pioneering work providing quantitative altitude profiles of ambient BC concentration from the troposphere to the lower stratosphere for the first time by using a well-characterized single-particle LII instrument.

Moteki and Kondo (2007) have experimentally shown that even thick coating on the BC core by low-volatility organic materials (glycerol and oleic acid) does not affect the single-particle LII signals from the BC core. They also provided physical interpretations of the observed LII and scattering signal waveforms of BC-containing particles using a numerical model simulating the time-dependent particle's properties in an intracavity laser beam.

Gao et al. (2007) developed a novel method to directly measure the time-dependent position of the particle translating across an intracavity Gaussian laser beam by using a position-sensitive multi-element scattering detector placed at one of the four optical detection channels in the SP2 instrument. The scattering signal waveform from the position-sensitive detector enables a reconstruction of the scattering amplitude of each particle before evaporation. The coating thickness on the BC core can be theoretically estimated from the scattering amplitude of the BC-containing particle before evaporation. Moteki and Kondo (2008) developed another method to estimate the time-dependent position of each scattering particle translating across a Gaussian laser beam from the normalized derivative of the scattering signal waveform. This method enables a single-particle quantification of coating thickness on the BC core without installing a multi-element photodetector instead of a single-element photodetector. Although the random measurement error in Moteki and Kondo (2008)'s method is more susceptible to background noise in scattering signal waveform than Gao et al. (2007)'s method, the former will also be practically advantageous as it enables a reconstruction of the time-dependent scattering cross section of BC-containing particle using only a signal waveform from a single light-scattering photodetector. Later, the time-dependent scattering cross section of each incandescing particle was found to help identify the morphological type (attached or coated type) of BC-containing particles (Moteki et al. 2014) as well as for categorizing incandescing iron oxide particles either of anthropogenic or desert dust origin (Moteki et al. 2017).

Moteki and Kondo (2010) characterized the LII-to-mass relationships for various BC samples using a newly available device for sorting the mass of aerosol particles accurately according to the balance between centrifugal and electrostatic forces acting on the aerosols (aerosol particle mass analyzer (APM); Ehara et al. 1996). APM enabled for the first time a sorting of aerosols by mass without particle shape-dependent bias and allowed the accurate calibration of single-particle LII instruments using non-spherical BC particles. Moteki and Kondo (2010) showed that the LII-to-mass relationship depends on both particle's refractive index and shape. The observed dependences were physically interpretable by the generalized Kirchhoff's law (Rytov 1953), as experimentally confirmed by Moteki et al. (2009) and Moteki et al. (2011). The linear proportionality between LII signal amplitude and BC mass, frequently assumed in SP2-related publications, is satisfied only if the radiation at the wavelengths used for incandescence detection (typically within 300–750 nm) can penetrate the entire volume of a BC particle if the radiation counterpropagating from the observation point incident onto the BC particle. This condition is satisfied when the size of BC aggregate is smaller than the wavelengths. In larger particle-size domains, the LII-to-mass relationship becomes nonlinear and strongly depends on the compactness of particle shape. Moteki and Kondo (2010) could not concretely demonstrate the dependence of the LII-to-mass linear slope to the BC refractive index at the smaller particle-size domain because of the several theoretical assumptions in their method for refractive index estimation (Moteki et al. 2010b). An experimental determination of the refractive index of BC at visible wavelengths has been one of the open problems in aerosol-climate sciences, which will be discussed again in Sect. 3.

Because of the similarity in LII-to-mass linear slope at the smaller size domain with ambient BC and diesel soot particles (Laborde et al. 2012) and the ease of particle generation, fullerene soot (Alfa Aesar Inc.) has

been recommended as a standard BC powder material for calibrating single-particle LII instruments (Baumgardner et al. 2012). At the larger particle-size domain (i.e., size > ~ LII wavelength), nonlinearity due to the shape effects should be considered. This consideration is crucial in measurements of BC mass concentration in rain and snow samples, wherein the BC size distributions tend to shift larger than in the atmosphere (e.g., Schwarz et al. 2013; Kinase et al. 2020; Mori et al. 2021).

The single-particle LII method is also able to detect light-absorbing iron oxides from desert dust (Liu et al. 2018) and anthropogenic combustion sources (e.g., vehicles) (Moteki et al. 2017; Ohata et al. 2018). Laboratory experiments showed that the particle's incandescence efficiency in a given operating laser power of black-colored iron oxides (magnetite and wüstite) is comparable to BC, whereas red-colored hematite showed lower efficiency. Notably, the LII-to-Fe-mass relationship was observed to be identical among wüstite, magnetite, and hematite (Yoshida et al. 2016; Mori et al. 2023). In addition, the LII signal's particle-size and spectral dependences agreed with the theoretical emission cross section according to Mie theory (Yoshida et al. 2018). These results suggest that each solid non-spherical particle consisting of any of wüstite (Fe(II)), magnetite (Fe(II, III)), and hematite (Fe(III)) has transformed into a molten iron (Fe) droplet in a laser beam before it starts to incandesce at boiling point (~ 3300 K). This fact allows theoretical extrapolation of the LII-to-Fe-mass relationship assuming spherical Fe particle beyond the upper particle mass limit sortable using the APM, that is, ~ 1000 fg or ~ 700 nm in volume-equivalent diameter (Yoshida et al. 2016; Mori et al. 2023). This extrapolation is essential in atmospheric measurements as most of the anthropogenic iron oxide mass concentration is distributed beyond ~ 700 nm volume-equivalent diameter (Moteki et al. 2017; Yoshida et al. 2020).

After the above development efforts over two decades, the single-particle LII method, also known as commercialized instrument SP2, has become a standard method for identifying and quantifying BC and BC-containing particles in the atmosphere essentially without the limit of lowest detectable number concentration. The single-particle LII with a nebulizer has also been the quantitative method for measuring BC in precipitated freshwater samples (e.g., rainwater, snowpack, ice sheets).

Corbin and Gysel-Beer et al. (2019) demonstrate the possibility of identifying strongly light-absorbing spherical BrC particles (i.e., tarball; Pósfai et al. 2004) using the single-particle LII.

2.3 Complex amplitude sensor

We briefly review another recent method for optical particle characterization, the complex amplitude sensor, which is useful for in-line BC measurements. The complex scattering amplitude $S = \mathrm{Re}S + i\mathrm{Im}S = |S|e^{i\Delta}$ represents the amplitude $|S|$ and phase shift Δ of the scattered field relative to those of the plane-wave field incident to the scattering particle (van de Hulst 1957). The S is a function of the angle θ between the incident beam and observation direction. The S reflects the physical properties of the scattering particle, such as refractive index, volume, shape, and orientation, and thus plays pivotal roles in optical particle characterizations and remote sensing of aerosols and clouds (Jones 1999; Romanov and Yurkin 2021). Light-scattering sensors, including the optical particle counters, nephelometers, and remote sensing methods for reflected and scattered radiations, are designed to measure the power of the scattered field $|S(\theta)|^2$ at $\theta \neq 0°$, avoiding the direct optical beam of the incident field. On the other hand, light extinction sensors, including occultation single-particle sensors, cavity-ringdown extinction spectroscopies, and remote sensing methods for direct radiation, are designed to measure the interference power of the scattered and incident fields in the forward direction $\mathrm{Im}S(0°)$ by monitoring the direct beam (Mishchenko 2014). Simultaneous measurement of both $\mathrm{Re}S$ and $\mathrm{Im}S$ of suspended single particles has not been possible until recently because of its technical difficulties, as reviewed in Moteki (2021).

The self-reference interferometry of a forward-scattered field of single particles excited by a focused Gaussian beam, proposed by Giglio and Potenza (2011) and demonstrated by Potenza et al. (2015), has been further refined by Moteki (2021) as a principle to be able to measure the complex forward-scattering amplitude $S(0°)$ of single particles in liquid flow. We refer to it as complex amplitude sensor/sensing (CAS). The theoretical principle and hardware requirements for CAS have been described in Moteki (2021). The single-particle $S(0°)$-measurements with CAS enable a rigorous optical characterization of single spherical non-absorbing particles, which have only two unknown parameters (i.e., the real part of refractive index and diameter). The single-particle $S(0°)$-measurements enable the identification and classification of different particle populations (e.g., black carbon, mineral dust, bacteria) coexisting in an environmental water sample, thanks to the sensitivity of the location of $S(0°)$-cluster to the difference in material properties (complex refractive index, shape) of the size-distributed particle population (Yoshida et al. 2022). Moteki (2020) proposed an algorithm to constrain each particle population's complex refractive index, shape, and volume-equivalent size distribution from a distinct

$S(0°)$-cluster. This algorithm has been further refined by Moteki et al. (2023) and used to constrain the real and imaginary parts of the refractive index of ambient BC, as to be detailed in Sect. 3.4.

3 Observational findings

3.1 BC in the global atmosphere

BC mass concentration in the atmosphere had been nearly unknown before the single-particle LII (SP2 and its modified versions) became available for field observations. Here, we review the basic knowledge of atmospheric BC revealed from the single-particle LII. BC mass mixing ratio in the midlatitude continental atmosphere shows a steep vertical gradient in the lower troposphere, decreasing from ~ 100 ng $(\text{kg air})^{-1}$ near the surface to ~ 1 − 10 ng $(\text{kg air})^{-1}$ in the middle troposphere (Schwarz et al. 2006). BC mass mixing ratio level could be ~ 10 times larger than this profile in the regions around large emission sources (e.g., East Asia) (Oshima et al. 2012; Kondo et al. 2016). BC mass mixing ratio in the remote Pacific ocean was within the range of ~ 0.1 − 10 ng $(\text{kg air})^{-1}$ with a weak vertical gradient in the lower-to-upper troposphere (Schwarz et al. 2010; Katich et al. 2018). BC mass mixing ratio over the remote Atlantic Ocean tends to be substantially higher than the Pacific Ocean due to the proximity to continental sources in midlatitudes and the strong influence of African biomass burning in tropical latitudes (Katich et al. 2018). The BC mass fraction was ~ 1–2% or less of the total submicron aerosol mass (Schwarz et al. 2006; Gao et al. 2022). BC mass mixing ratio in the tropical tropopause layer, which is a gateway of injection of tropospheric aerosols into the stratosphere, was found to be ~ 1 ng $(\text{kg air})^{-1}$ (Gao et al. 2008), which was similar to the average value in the upper troposphere to lower stratosphere over the midlatitude (Schwarz et al. 2006). The global atmospheric BC data from the surface to upper troposphere are essential to evaluate the model assumptions on the emission and transport processes, as the new atmospheric BC dataset had revealed the model bias of a factor of ~ 10 or more in remote regions and higher altitudes (e.g., Koch et al. 2009; Wang et al. 2014; Katich et al. 2018). The observational datasets of BC mass mixing ratio in the global troposphere play critical roles in testing the assumptions of the parameters controlling the BC lifetime (e.g., the timescale of hydrophobic to hygroscopic conversion, in-cloud scavenging efficiency) in global models (Kipling et al. 2013; Hodnebrog et al. 2014; Lund et al. 2018; Liu and Matsui 2021).

Particle-size distribution of BC mass mixing ratio is approximated well with a log-normal distribution with the mode at ~ 200 ± 50 nm volume-equivalent BC core diameter, being reasonably independent of location and altitude up to the lower stratosphere (Schwarz et al. 2008a, 2010; Spackman et al. 2010; Kondo et al. 2011a; Laborde et al. 2013; Reddington et al. 2013; Schulz et al. 2019; Yang et al. 2019; Yoshida et al. 2020; Ohata et al. 2021b). Even though fresh urban plumes could exhibit smaller BC core size distribution < ~ 150 nm (Schwarz et al. 2008a; Laborde et al. 2013), the smaller distribution near the urban area will be of minor significance in regional-to-global scale as it transforms via coagulations to the stable distribution with the mode at ~ 200 nm in ~ 1 day after emission (Moteki et al. 2007; Miyakawa et al. 2017). Simultaneous observations of BC core size distribution in the atmosphere and rainwater provided observational evidence of the predominance of nucleation scavenging as a process controlling the efficiency of wet removal of submicron aerosols (Ohata et al. 2016; Moteki et al. 2019). Preferential removal of larger aerosol particles (with less critical supersaturation) through moist convections tends to shift the BC size distribution to smaller in cleaner, particle-free air masses (Moteki et al. 2012; Taylor et al. 2014; Schulz et al. 2019). The two opposite size-regulating processes control the size distribution of BC in the atmosphere: the coagulation growth in the dense plumes just after emission and the preferential removal of larger BC through cloud-precipitation processes.

The number fraction of internally mixed BC particles, as well as the thickness of the coating on the BC core (evaluated at ~ 200 nm BC core size), showed marked contrast between fresh urban plumes and fresh biomass-burning plumes: Thickly coated BC particles are far more dominant in biomass-burning plumes (Schwarz et al. 2008b; Kondo et al. 2011a). The thickness of the coating on BC particles in a fresh urban plume was found to increase with the production of secondary aerosols (e.g., sulfate and organics) as the plume ages in the atmosphere (Moteki et al. 2007; Shiraiwa et al. 2007; Miyakawa et al. 2017). The average coating thickness (evaluated at ~ 200 nm BC core diameter) was larger in the upper troposphere to lower stratosphere than in the lower-to-middle troposphere (Schwarz et al. 2008a). BC coating thickness over the Arctic region, dominated by a mixture of aged and cloud-processed aerosols, was approximately independent of altitude from the surface to ~ 5 km (Kodros et al. 2018; Ohata et al. 2021b). The degree of internal mixing of BC tends to be positively correlated with the total aerosol mass to BC mass ratio, which is an indicator of secondary aerosol production in the urban plume or the degree of contribution of the biomass-burning plume (Schwarz et al. 2008a, b; Moteki et al. 2014). Moteki et al. (2014) developed a method to classify the morphology of BC-containing particles into coated type and attached type according to the single-particle LII

signals. They found that the number fraction of attached type was only ~ 1% even in fresh urban air (Adachi et al. 2016), suggesting that the attached-type BC-containing particles are negligible in the atmosphere. Recent reanalyses of worldwide ground-based observation datasets revealed that the coating thickness of BC-containing particles universally follows exponential distributions, the parameters of which were pretty independent of BC core size and location (Wang et al. 2022). This suggests a possibility of a succinct but accurate representation of the BC mixing state in global aerosol models.

Observational results on microphysical properties of BC-containing particles obtained by the single-particle LII have been used for testing the recent aerosol models that explicitly simulate the BC aging process (Oshima et al. 2009; Matsui et al. 2013; Oshima and Koike 2013). Simulation accuracy of particle-size distribution and mixing state of BC is of fundamental importance for predicting atmospheric BC burden and its radiative effects, as the aging and cloud-droplet activation parameterizations are considered to be significant sources of uncertainty (Textor et al. 2006; Vignati et al. 2010; Moteki et al. 2019; Yu et al. 2019a, b; Holopainen et al. 2020; Matsui and Moteki 2020).

The new observational results obtained by the single-particle LII have also been used for updating the aerosol optical models for remote sensing algorithms (Schuster et al. 2022).

3.2 Comparison of single-particle LII with other BC measurements

The thermal-optical and filer-based light absorption methods were two primary techniques used for measuring BC mass concentration in ambient air, snow, and ice samples before the invention of single-particle LII. A notable advantage of thermal-optical and filter-based light absorption methods compared with the single-particle LII is their applicability to BC samples with any particle-size range. Pileci et al. (2021) reported that ambient-mass concentrations of refractory carbon derived from thermal-optical and single-particle LII methods could differ within a factor of ~ 2. The BC measurement bias in filter-based light absorption methods can be largely suppressed by removing volatile aerosol components using a heated aerosol inlet (Kondo et al. 2009; Irwin et al. 2013; Ohata et al. 2019), as demonstrated in fresh urban pollutions (Kondo et al. 2011b) and Arctic atmosphere (Ohata et al. 2021a).

3.3 Anthropogenic iron oxide

The in situ aerosol measurements using single-particle LII and laboratory analyses of collected aerosol samples using a transmission electron microscope (TEM) revealed that anthropogenic light-absorbing iron oxides (FeOx) consisting of an aggregate of magnetite nanoparticles are ubiquitous in the urban plumes and the East Asian and Arctic troposphere (Moteki et al. 2017; Ohata et al. 2018; Yoshida et al. 2018). The mass mixing ratio of anthropogenic FeOx in these regions was ~ 20–60% of BC (Yoshida et al. 2020). The anthropogenic FeOx aerosol is likely ubiquitous in the global troposphere (Lamb et al. 2021) and will be one of the contributors to regional-to-global-scale aerosol's shortwave absorption (Moteki et al. 2017; Matsui et al. 2018; Ito et al. 2018). These new observation data provided further evidence to constrain the magnitude and spatial distribution of anthropogenic Fe emission (Rathod et al. 2020; Liu et al. 2022), which is an essential factor for investigating the effects of Fe-bearing aerosols on ocean fertilization (Hamilton et al. 2020; Ito et al. 2021).

3.4 BC refractive index

The complex refractive index $m = m_r + im_i$ is possibly the most critical climate-relevant property of atmospheric aerosols as it largely determines the efficiency of absorption and scattering of solar radiation by particles. Refractive indices of non-light-absorbing aerosol materials (e.g., sulfate, organics, aluminosilicates, sea salt) at visible wavelengths are around $m_r \sim 1.5 \pm 0.05$ under dry conditions. By contrast, refractive indices of insoluble light-absorbing materials (BC, iron oxides, insoluble BrC) are still not sufficiently known.

Experimental determination of the refractive index of a particulate material always requires a close comparison between rigorous light-scattering theory and accurate optical measurements. The theory-to-measurement comparisons have been technically challenging for BC aggregates in the atmosphere due to their wavelength-scale irregularity of particle shape and mixing with other aerosol components.

Currently, assumptions of BC refractive index at visible wavelengths are mostly chosen between the lower and upper limits recommended by Bond and Bergstrom (2006), $1.75 + 0.63i$ (BB06-l) and $1.95 + 0.79i$ (BB06-h), respectively. The recommendation was based on a compilation of experimental results for synthetic BC samples (e.g., propane–oxygen flame soot, carbon black) obtained earlier than the early-2000s. The validity of the BB06 is still being determined as experimental methods in the early-2000s include various assumptions (e.g., spherical BC shape). The refractive index of atmospheric BC material could be variable and different from any synthetic carbon material.

Liu et al. (2020b) pointed out that the theoretically computed mass absorption cross section (MAC, m^2/g) of uncoated BC aggregates using BB06 refractive indices

underestimated the experimental MAC values by ~ 30%. This systematic discrepancy suggests that further investigations on BC refractive index are still needed.

Moteki (2020) proposed a method for estimating the refractive index of waterborne particles from the measured distribution in complex forward-scattering amplitude $S(0°)$. Moteki et al. (2023) improved this approach using an updated $S(0°)$-measurement protocol (Moteki 2021) and a more sophisticated inverse-scattering model for BC aggregates. They applied the method to constrain the ambient BC refractive index collected from the atmosphere over the northwestern Pacific Ocean at 633 nm wavelength. From the new $S(0°)$ data for atmospheric BC and recently reported MAC values for various types of flame-generated BC, Moteki et al. (2023) constrained a plausible (m_r, m_i) domain that contains the BC refractive index at 633 nm wavelength:

$$\begin{cases} 0.51 + 0.014 m_r^{5.2} \le m_i \le 2.5 m_r - 3.5 \text{ if } 1.7 \le m_r \le 1.8 \\ 0.51 + 0.014 m_r^{5.2} \le m_i \le 1.5 \text{ if } 1.8 < m_r \le 2.2. \end{cases}$$

Even though the BB06 values are currently "accepted" in the climate and atmospheric science community, they are located outside the plausible (m_r, m_i) domain constrained from the new experimental evidence. The persistent ~ 30% underpredictions of MAC using the BB06-l or BB06-h value pointed out by Liu et al. (2020b) will be mitigated if its imaginary part is increased to a value inside the suggested (m_r, m_i) domain.

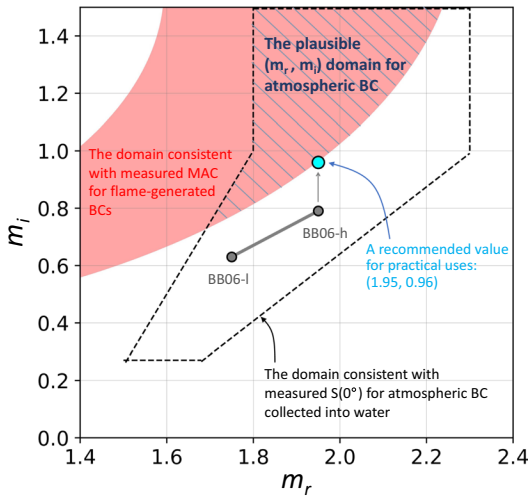

Fig. 2 Illustrating the three-different (m_r, m_i) domains for the complex refractive index of BC.: 1) The domain consistent with measured $S(0°)$ for atmospheric BC (enclosed by black-dashed lines), 2) the domain consistent with measured MAC for various flame-generated BCs (red-filled area), and 3) the domain constrained by both MAC- and S(0°)-measurements (Moteki et al. 2023). The conventional assumptions BB06-l (1.75 + 0.63i) and BB06-h (1.95 + 0.79i) (gray-filled circles) and the recommendable value for practical uses 1.95 + 0.96i (blue-filled circle) suggested by Moteki et al. (2023) are also plotted

For straightforward applications of the new constraint of BC refractive index by climate and atmospheric research, Moteki et al. (2023) suggested a recommendable $m_r + m_i$ value from the constrained (m_r, m_i) domain, 1.95 + 0.96i, which was determined by increasing the imaginary part of the BB06-h to the lower m_i boundary of the plausible (m_r, m_i) domain (Fig. 2). Assuming the 1.95 + 0.96i instead of the BB06-h (1.95 + 0.79i) will result in a ~ 16% increase of calculated shortwave absorption by BC-containing aerosols. This implies a non-negligible underestimate of shortwave absorption by black carbon aerosols in current climate simulations using BB06-h.

4 Open problems and suggestions

4.1 BC measurement techniques

The most important open issue of the current single-particle LII technique is the uncertainty or difficulty of measuring BC particles much larger than the visible wavelengths. Current commercial single-particle LII instruments (e.g., SP2 from Droplet Measurement Technologies, Inc.) are designed to detect BC core within ~ 70–500 nm volume-equivalent diameter. The NOAA SP2 instruments used for global-scale aircraft observations were intended to measure ~ 70–550 nm BC core (Schwarz et al. 2010; Katich et al. 2018). Aircraft and ground observations using the single-particle LII instrument of The University of Tokyo (a modified version of SP2; Moteki and Kondo 2010), which detects 70–850 nm BC core, indicated a non-negligible contribution of BC with > ~ 500 nm diameter to size-integrated BC mass mixing ratio (Kondo et al. 2016; Yoshida et al. 2020). This implies the significance of extending the upper limit of the BC core size range observable by single-particle LII instruments at least up to ~ 1000 nm. The importance of extending the LII-detectable particle-size range is even more evident for FeOx (Moteki et al. 2017; Lamb et al. 2021). The author therefore suggests fundamental investigations for extending the upper limit of the observable particle-size range in the single-particle LII.

Another important open issue on the current BC measurement technique is the lack of measurement principles applicable to various types of sample fluids. For example, single-particle LII is currently not able to apply to the BC particles suspended in high-solute concentration fluids such as ocean water. One of the unique advantages of the CAS compared with single-particle LII is its applicability to in situ single-particle measurements of any insoluble particles suspended in any transparent liquids (e.g., freshwater, ocean water, organic solvents). The CAS is a potential tool for in situ real-time measurements of BC in ocean water. In addition, the CAS will be able to

measure both BC and mineral dust particles coexisting in an environmental water sample (Yoshida et al. 2022). The author suggests investigations on CAS technique to be able to use it for in-line measurement of size-resolved number concentrations of BC particles in various types of environmental fluids. Before the wide applications, consistencies in the quantified physical properties (e.g., BC mass) between single-particle LII and CAS should also be established.

4.2 BC outside the troposphere

Observational understandings of BC outside the troposphere still need to be improved. BC exerts stronger radiative effects per unit mass in the stratosphere than in the troposphere due to its longer lifetime and higher actinic flux. It was known that biomass-burning (BB) plumes from wildfires could penetrate the tropopause and intrude into the lower stratosphere through strong convective systems (Jost et al. 2004; Ansmann et al. 2018). Sporadic intrusions of BB plumes enhance the annual mean BC mass mixing ratio of the lowermost stratosphere over Europe and North America by about ~ 75% from the regional background (Ditas et al. 2018). Strong shortwave absorption by BC drives buoyant uplift of the injected plumes in the stratosphere (Yu et al. 2019b, 2021; Gao et al. 2021). Further understanding of the origins, physicochemical properties, and removal processes of stratospheric aerosols are needed (Kremser et al. 2016; Murphy et al. 2021) to predict the effects and side-effects of the stratospheric aerosol injection for solar radiation management (e.g., Niemeier and Timmreck 2015). The author suggests that in situ BC measurements in the stratosphere help to develop the fundamental understanding as BC is an inert particle tracer of combustion-originated tropospheric materials.

BC in the cryosphere has been actively investigated for its importance as a climate forcer and as a proxy of historical environmental changes (Kang et al. 2020). BC embedded in the ice sheets can provide information on the historical record of atmospheric concentration of combustion-induced aerosols (e.g., McConnell et al. 2007; Winstrup et al. 2019). BC significantly contributes to snow albedo reduction in polar regions and midlatitude glaciers (Flanner et al. 2007; Skiles et al. 2018). It was estimated that BC is the second largest contributor to positive radiative forcing among all the anthropogenic gases and aerosols in Arctic regions due mainly to its effects on snow albedo reduction (Oshima et al. 2020). However, the interpretation of BC-in-snow observations is still controversial due to the complex processes that affect BC concentration and microphysical properties after deposition (e.g., Schmitt et al. 2019). Particle-size distribution of BC-in-snow and BC-in-glacier tends to be substantially larger than the BC-in-atmosphere for unknown physical mechanisms (Schwarz et al. 2013; Zhang et al. 2017; Mori et al. 2019; Kinase et al. 2020). The larger shift of BC size distribution might cause an underestimate of BC mass concentration measured by some commercial single-particle LII instruments without extending the detectable BC size range. The author suggests the importance of further improvements of BC measurement techniques for snow and ice-sheet samples in terms of accuracy and ease of operation. That should help to accelerate understanding of the physical properties and processes of BC in the cryosphere.

BC is persistent in the natural environment on timescales of centuries to millennia (Goldberg 1985). Occurrences of wildfires and burnings of fossil fuel and biofuel modify the turnover rate of the global carbon cycle by converting relatively labile organic carbon to more environmentally persistent, slowly cycling BC (Coppola et al. 2022). A large fraction of BC particles emitted into the atmosphere will be input into the ocean. BC is the largest slow-cycling organic carbon reservoir in the ocean (e.g., Yamashita et al. 2022). The current standard analytical methods for BC in ocean water were designed to quantify the dissolved refractory aromatic molecules (dissolved BC) (e.g., Dittmar 2008), which is different from the analytical methods for particulate BC in the atmosphere (Coppola et al. 2022). A quantitative estimate of the oceanic BC budget requires atmospheric BC data (Bao et al. 2017). However, the consistency of the current BC datasets available from atmospheric and oceanic disciplines is nearly unknown. The author suggests that the CAS would help to provide consistent particulate BC datasets in the atmosphere, cryosphere, and ocean.

5 Conclusive remarks

We reviewed recent advances in in situ measurement methods and observational findings since the mid-2000s on atmospheric BC aerosol, one of the most important short-lived climate forcers. Quantification of climate-relevant properties of atmospheric BC and BC-containing particles has been continually updated over two decades. The single-particle LII has been playing an important role in field observations and observation-based updates of assumptions in climate models and remote sensing algorithms. Although the global anthropogenic BC emission from fossil fuel burning is expected to decrease owing to the clean air act, natural BC emissions from wildfires and the occurrence of BC injection to the stratosphere may increase globally with greenhouse gas-induced climate change. Further developments in the measurement methods and observational knowledge on environmental BC should help improve the predictabilities of short-term

climate response to atmospheric composition and the long-term global carbon cycle.

Abbreviations

BC	Black carbon
BrC	Brown carbon
OC	Organic carbon
FeOx	Iron oxides
LII	Laser-induced incandescence
SP2	Single-particle soot photometer
CAS	Complex amplitude sensor

Acknowledgements
The author acknowledges the Japan Geoscience Union for this opportunity to write a review paper focused on the author's research area.

Author contributions
NM conceived the research idea and wrote the manuscript. The author read and approved the final manuscript.

Funding
Funds were provided by the Environment Research and Technology Development Fund (JPMEERF20202003) of the Environmental Restoration and Conservation Agency, the Japan Society for the Promotion of Science (JSPS) KAKENHI program (JP19H04236, JP19KK0289, JP19H04259, JP19H05699, 22H03722, and 22H01294), and the Arctic Challenge for Sustainability ArCS II project (JPMXD1420318865) of the Ministry of Education, Culture, Sports, Science, and Technology (MEXT) of Japan.

Availability of data and materials
Not applicable.

Declarations

Competing interests
The authors declare that they have no competing interests.

Received: 11 January 2023 Accepted: 28 February 2023
Published: 6 March 2023

References

Adachi K, Moteki N, Kondo Y, Igarashi Y (2016) Mixing states of light-absorbing particles measured using a transmission electron microscope and a single-particle soot photometer in Tokyo. Jpn J Geophys Res Atmos 121(15):9153–9164. https://doi.org/10.1002/2016jd025153

Andreae MO, Gelencsér A (2006) Black carbon or brown carbon? the nature of light-absorbing carbonaceous aerosols. Atmos Chem Phys 6(10):3131–3148. https://doi.org/10.5194/acp-6-3131-2006

Ansmann A, Baars H, Chudnovsky A, Mattis I, Veselovskii I, Haarig M, Seifert P, Engelmann R, Wandinger U (2018) Extreme levels of Canadian wildfire smoke in the stratosphere over central Europe on 21–22 August 2017. Atmos Chem Phys 18(16):11831–11845. https://doi.org/10.5194/acp-18-11831-2018

Apicella B, Ciajolo A, Tregrossi A, Abrahamson J, Vander Wal RL, Russo C (2018) HRTEM and EELS investigations of flame-formed soot nanostructure. Fuel 225:218–224. https://doi.org/10.1016/j.fuel.2018.03.091

Axelsson B, Collin R, Bengtsson PE (2000) Laser-induced incandescence for soot particle size measurements in premixed flat flames. Appl Opt 39(21):3683–3690. https://doi.org/10.1364/ao.39.003683

Bao H, Niggemann J, Luo L, Dittmar T, Kao SJ (2017) Aerosols as a source of dissolved black carbon to the ocean. Nat Commun 8(1):510. https://doi.org/10.1038/s41467-017-00437-3

Baumgardner D, Kok G, Raga G (2004) Warming of the Arctic lower stratosphere by light absorbing particles. Geophys Res Lett 31:L06117. https://doi.org/10.1029/2003gl018883

Baumgardner D, Popovicheva O, Allan J, Bernardoni V, Cao J, Cavalli F, Cozic J, Diapouli E, Eleftheriadis K, Genberg PJ, Gonzalez C, Gysel M, John A, Kirchstetter TW, Kuhlbusch TAJ, Laborde M, Lack D, Müller T, Niessner R, Petzold A, Piazzalunga A, Putaud JP, Schwarz J, Sheridan P, Subramanian R, Swietlicki E, Valli G, Viana M (2012) Soot reference materials for instrument calibration and intercomparisons: a workshop summary with recommendations. Atmos Meas Tech 5(8):1869–1887. https://doi.org/10.5194/amt-5-1869-2012

Bhandari J, China S, Chandrakar KK, Kinney G, Cantrell W, Shaw RA, Mazzoleni LR, Girotto G, Sharma N, Gorkowski K, Gilardoni S, Decesari S, Facchini MC, Zanca N, Pavese G, Esposito F, Dubey MK, Aiken AC, Chakrabarty RK, Moosmüller H, Onasch TB, Zaveri RA, Scarnato BV, Fialho P, Mazzoleni C (2019) Extensive soot compaction by cloud processing from laboratory and field observations. Sci Rep 9(1):11824. https://doi.org/10.1038/s41598-019-48143-y

Bond TC, Bergstrom RW (2006) Light absorption by carbonaceous particles: an investigative review. Aerosol Sci Technol 40(1):27–67. https://doi.org/10.1080/02786820500421521

Bond TC, Anderson TL, Campbell D (1999) Calibration and intercomparison of filter-based measurements of visible light absorption by aerosols. Aerosol Sci Technol 30(6):582–600. https://doi.org/10.1080/027868299304435

Bond TC, Doherty SJ, Fahey DW, Forster PM, Berntsen T, DeAngelo BJ, Flanner MJ, Ghan S, Kärcher B, Koch D, Kinne S, Kondo Y, Quinn PK, Sarofim MC, Schultz MG, Schulz M, Venkataraman C, Zhang H, Zhang N, Bellouin N, Guttikunda SK, Hopke PK, Jacobson MZ, Kaiser JW, Klimont Z, Lohmann U, Schwarz JP, Shindell D, Storelvmo T, Warren SG, Zender CS (2013) Bounding the role of black carbon in the climate system: a scientific assessment. J Geophys Res Atmos 118(11):5380–5552. https://doi.org/10.1002/jgrd.50171

Buseck PR, Adachi K, Gelencsér A, Tompa É, Pósfai M (2014) Ns-soot: a material-based term for strongly light-absorbing carbonaceous particles. Aerosol Sci Technol 48(7):777–788. https://doi.org/10.1080/02786826.2014.919374

Cavalli F, Viana M, Yttri KE, Genberg J, Putaud JP (2010) Toward a standardised thermal-optical protocol for measuring atmospheric organic and elemental carbon: the EUSAAR protocol. Atmos Meas Tech 3(1):79–89. https://doi.org/10.5194/amt-3-79-2010

Coppola AI, Wagner S, Lennartz ST, Seidel M, Ward ND, Dittmar T, Santín C, Jones MW (2022) The black carbon cycle and its role in the earth system. Nat Rev Earth Environ 3(8):516–532. https://doi.org/10.1038/s43017-022-00316-6

Corbin JC, Gysel-Beer M (2019) Detection of tar brown carbon with a single particle soot photometer (SP2). Atmos Chem Phys 19(24):15673–15690. https://doi.org/10.5194/acp-19-15673-2019

Corbin JC, Czech H, Massabò D, de Mongeo FB, Jakobi G, Liu F, Lobo P, Mennucci C, Mensah AA, Orasche J, Pieber SM, Prévôt ASH, Stengel B, Tay LL, Zanatta M, Zimmermann R, El Haddad I, Gysel M (2019) Infrared-absorbing carbonaceous tar can dominate light absorption by marine-engine exhaust. Npj Clim Atmos Sci 2:12. https://doi.org/10.1038/s41612-019-0069-5

Ditas J, Ma N, Zhang Y, Assmann D, Neumaier M, Riede H, Karu E, Williams J, Scharffe D, Wang Q, Saturno J, Schwarz JP, Katich JM, McMeeking GR, Zahn A, Hermann M, Brenninkmeijer M, Andreae MO, Pöschl U, Su H, Cheng Y (2018) Strong impact of wildfires on the abundance and aging of black carbon in the lowermost stratosphere. Proc Natl Acad Sci U S A 115(50):E11595–E11603. https://doi.org/10.1073/pnas.1806868115

Dittmar T (2008) The molecular level determination of black carbon in marine dissolved organic matter. Org Geochem 39(4):396–407. https://doi.org/10.1016/j.orggeochem.2008.01.015

Dusek U, Reischl GP, Hitzenberger R (2006) CCN activation of pure and coated carbon black particles. Environ Sci Technol 40(4):1223–1230. https://doi.org/10.1021/es0503478

Ehara K, Hagwood C, Coakley KJ (1996) Novel method to classify aerosol particles according to their mass-to-charge ratio—aerosol particle mass analyser. J Aerosol Sci 27(2):217–234. https://doi.org/10.1016/0021-8502(95)00562-5

Ervens BT, Turpin BJ, Weber RJ (2011) Secondary organic aerosol formation in cloud droplets and aqueous particles (aqSOA): a review of laboratory, field and model studies. Atmos Chem Phys 11(21):11069–11102. https://doi.org/10.5194/acp-11-11069-2011

Flanner MG, Zender CS, Randerson JT, Rasch PJ (2007) Present-day climate forcing and response from black carbon in snow. J Geophys Res. https://doi.org/10.1029/2006jd008003

Fuller KA, Malm WC, Kreidenweis SM (1999) Effects of mixing on extinction by carbonaceous particles. J Geophys Res 104(D13):15941–15954. https://doi.org/10.1029/1998jd100069

Gao RS, Schwarz JP, Kelly KK, Fahey DW, Watts LA, Thompson TL, Spackman JR, Slowik JG, Cross ES, Han JH, Davidovits P, Onasch TB, Worsnop DR (2007) A novel method for estimating light-scattering properties of soot aerosols using a modified single-particle soot photometer. Aerosol Sci Technol 41(2):125–135. https://doi.org/10.1080/02786820601118398

Gao RS, Hall SR, Swartz WH, Schwarz JP, Spackman JR, Watts LA, Fahey DW, Aikin KC, Shetter RE, Bui TP (2008) Calculations of solar shortwave heating rates due to black carbon and ozone absorption using in situ measurements. J Geophys Res 113:D14203. https://doi.org/10.1029/2007jd009358

Gao RS, Rosenlof KH, Kärcher B, Tilmes S, Toon OB, Maloney C, Yu P (2021) Toward practical stratospheric aerosol albedo modification: solar-powered lofting. Sci Adv 7(20):eabe3416. https://doi.org/10.1126/sciadv.abe3416

Gao CY, Heald CL, Katich JM, Luo G, Yu F (2022) Remote aerosol simulated during the atmospheric tomography (ATom) campaign and implications for aerosol lifetime. J Geophys Res Atmos 127(22):e2022JD036524. https://doi.org/10.1029/2022JD036524

Giglio M, Potenza MAC (2011) Method of measuring properties of particles and corresponding apparatus. US Patent 7924431B2. issued April 12, 2011.

Goldberg ED (1985) Black carbon in the environment: properties and distribution. John Wiley and Sons, New York

Goulay F, Schrader PE, Nemes L, Dansson MA, Michelsen HA (2009) Photochemical interferences for laser-induced incandescence of flame-generated soot. Proc Combust Inst 32(1):963–970. https://doi.org/10.1016/j.proci.2008.05.030

Hamilton DS, Scanza RA, Rathod SD, Bond TC, Kok JF, Li L, Matsui H, Mahowald NM (2020) Recent (1980 to 2015) trends and variability in daily-to-interannual soluble iron deposition from dust, fire, and anthropogenic sources. Geophys Res Lett 47(17):e2020GL089688. https://doi.org/10.1029/2020gl089688

Hodnebrog Ø, Myhre G, Samset BH (2014) How shorter black carbon lifetime alters its climate effect. Nat Commun 5(1):5065. https://doi.org/10.1038/ncomms6065

Holopainen E, Kokkola H, Laakso A, Kühn T (2020) In-cloud scavenging scheme for sectional aerosol modules—implementation in the framework of the sectional aerosol module for large scale applications version 2.0 (SALSA2.0) global aerosol module. Geosci Model Dev 13(12):6215–6235. https://doi.org/10.5194/gmd-13-6215-2020

Irwin M, Kondo Y, Moteki N, Miyakawa T (2013) Evaluation of a heated-inlet for calibration of the SP2. Aerosol Sci Technol 47(8):895–905. https://doi.org/10.1080/02786826.2013.800187

Ito A, Lin G, Penner JE (2018) Radiative forcing by light-absorbing aerosols of pyrogenetic iron oxides. Sci Rep 8:7347. https://doi.org/10.1038/s41598-018-25756-3

Ito A, Ye Y, Baldo C, Shi Z (2021) Ocean fertilization by pyrogenic aerosol iron. Npj Clim Atmos Sci 4:30. https://doi.org/10.1038/s41612-021-00185-8

Jones AR (1999) Light scattering for particle characterization. Prog Energy Combust Sci 25(1):1–53. https://doi.org/10.1016/s0360-1285(98)00017-3

Jost HJ, Drdla K, Stohl A, Pfister L, Loewenstein M, Lopez JP, Hudson PK, Murphy DM, Cziczo DJ, Fromm M, Bui P, Dean-Day J, Gerbig C, Mahoney MJ, Richard EC, Spichtinger N, Pittman JV, Weinstock EM, Wilson JC, Xueref I (2004) In-situ observations of mid-latitude forest fire plumes deep in the stratosphere. Geophys Res Lett 31:L11101. https://doi.org/10.1029/2003gl019253

Kalberer M, Paulsen D, Sax M, Steinbacher M, Dommen J, Prévôt AS, Fisseha R, Weingartner E, Frankevich V, Zenobi R, Baltensperger U (2004) Identification of polymers as major components of atmospheric organic aerosols. Science 303(5664):1659–1662. https://doi.org/10.1126/science.1092185

Kanakidou M, Seinfeld JH, Pandis SN, Barnes I, Dentener FJ, Facchini MC, Dingenen RV, Ervens B, Nenes A, Nielsen CJ, Swietlicki E, Putaud JP, Balkanski Y, Fuzzi S, Horth J, Moortgat GK, Winterhalter R, Myhre CEL, Tsigaridis K, Vignati E, Stephanou EG, Wilson J (2005) Organic aerosol and global climate modelling: a review. Atmos Chem Phys 25(4):1053–1123. https://doi.org/10.5194/acp-5-1053-2005

Kang S, Zhang Y, Qian Y, Wang H (2020) A review of black carbon in snow and ice and its impact on the cryosphere. Earth Sci Rev 210:103346. https://doi.org/10.1016/j.earscirev.2020.103346

Karanasiou A, Minguillón MC, Viana M, Alastuey A, Putaud JP, Maenhaut W, Panteliadis P, Močnik G, Favez O, Kuhlbusch TA (2015) Thermal-optical analysis for the measurement of elemental carbon (EC) and organic carbon (OC) in ambient air a literature review. Atmos Meas Tech Discuss 8(9):9649–9712. https://doi.org/10.5194/amtd-8-9649-2015

Kasper G (1982) Dynamics and measurement of smokes. I size characterization of nonspherical particles. Aerosol Sci Technol 1(2):187–199. https://doi.org/10.1080/02786828208958587

Katich JM, Samset BH, Bui TP, Dollner M, Froyd KD, Campuzano-Jost P, Nault BA, Schroder JC, Weinzierl B, Schwarz JP (2018) Strong contrast in remote black carbon aerosol loadings between the Atlantic and pacific basins. J Geophys Res Atmos 123(23):13386–13395. https://doi.org/10.1029/2018jd029206

Kazemimanesh M, Rahman MM, Duca D, Johnson TJ, Addad A, Giannopoulos G, Focsa C, Boies AM (2022) A comparative study on effective density, shape factor, and volatile mixing of non-spherical particles using tandem aerodynamic diameter, mobility diameter, and mass measurements. J Aerosol Sci 161:105930. https://doi.org/10.1016/j.jaerosci.2021.105930

Kinase T, Adachi K, Oshima N, Goto-Azuma K, Ogawa-Tsukagawa Y, Kondo Y, Moteki N, Ohata S, Mori T, Hayashi M, Hara K, Kawashima H, Kita K (2020) Concentrations and size distributions of black carbon in the surface snow of eastern Antarctica in 2011. J Geophys Res Atmos 125:e2019JD03073. https://doi.org/10.1029/2019jd030737

Kipling Z, Stier P, Schwarz JP, Perring A, Spackman JR, Mann GW, Johnson CE, Telford PJ (2013) Constraints on aerosol processes in climate models from vertically-resolved aircraft observations of black carbon. Atmos Chem Phys 13(12):5969–5986. https://doi.org/10.5194/acp-13-5969-2013

Knutson EO, Whitby KT (1975) Aerosol classification by electric mobility: apparatus, theory, and applications. J Aerosol Sci 6(6):443–451. https://doi.org/10.1016/0021-8502(75)90060-9

Koch D, Schulz M, Kinne S, McNaughton C, Spackman JR, Balkanski Y, Bauer S, Berntsen T, Bond TC, Boucher O, Chin M, Clarke A, De Luca N, Dentener F, Diehl T, Dubovik O, Easter R, Fahey DW, Feichter J, Fillmore D, Freitag S, Ghan S, Ginoux P, Gong S, Horowitz L, Iversen T, Kirkevåg A, Klimont Z, Kondo Y, Krol M, Liu X, Miller R, Montanaro V, Moteki N, Myhre G, Penner JE, Perlwitz J, Pitari G, Reddy S, Sahu L, Sakamoto H, Schuster G, Schwarz JP, Seland Ø, Stier P, Takegawa N, Takemura T, Textor TC, van Aardenne JA, Zhao Y (2009) Evaluation of black carbon estimations in global aerosol models. Atmos Chem Phys 9(22):9001–9026. https://doi.org/10.5194/acp-9-9001-2009

Kodros JK, Hanna SJ, Bertram AK, Leaitch WR, Schulz H, Herber AB, Zanatta M, Burkart J, Willis MD, Abbatt JPD, Pierce JR (2018) Size-resolved mixing state of black carbon in the Canadian high Arctic and implications for simulated direct radiative effect. Atmos Chem Phys 18(15):11345–11361. https://doi.org/10.5194/acp-18-11345-2018

Kondo Y, Sahu L, Kuwata M, Miyazaki Y, Takegawa N, Moteki N, Imaru J, Han S, Nakayama T, Kim Oanh NT, Hu M, Kim YJ, Kita K (2009) Stabilization of the mass absorption cross section of black carbon for filter-based absorption photometry by the use of a heated inlet. Aerosol Sci Technol 43(8):741–756. https://doi.org/10.1080/02786820902889879

Kondo Y, Matsui H, Moteki N, Sahu L, Takegawa N, Kajino M, Zhao Y, Cubison MJ, Jimenez JL, Vay S, Diskin GS, Anderson B, Wisthaler A, Mikoviny T, Fuelberg HE, Blake DR, Huey G, Weinheimer AJ, Knapp DJ, Brune WH (2011a) Emissions of black carbon, organic, and inorganic aerosols from biomass burning in North America and Asia in 2008. J Geophys Res 116:D08204. https://doi.org/10.1029/2010jd015152

Kondo Y, Sahu L, Moteki N, Khan F, Takegawa N, Liu X, Koike M, Miyakawa T (2011b) Consistency and traceability of black carbon measurements made by laser-induced incandescence, thermal-optical transmittance, and filter-based photo-absorption techniques. Aerosol Sci Technol 45(2):295–312. https://doi.org/10.1080/02786826.2010.533215

Kondo Y, Moteki N, Oshima N, Ohata S, Koike M, Shibano Y, Takegawa N, Kita K (2016) Effects of wet deposition on the abundance and size distribution

of black carbon in East Asia. J Geophys Res Atmos 121(9):4691–4712. https://doi.org/10.1002/2015jd024479
Kremser S, Thomason LW, von Hobe M, Hermann M, Deshler T, Timmreck C, Toohey M, Stenke A, Schwarz JP, Weigel R, Fueglistaler S, Prata FJ, Vernier JP, Schlager H, Barnes JE, Antuña-Marrero JC, Fairlie D, Palm M, Mahieu E, Notholt J, Rex M, Bingen C, Vanhellemont F, Bourassa A, Plane JMC, Klocke D, Carn SA, Clarisse L, Trickl T, Neely R, James AD, Rieger L, Wilson JC, Meland B (2016) Stratospheric aerosol-Observations, processes, and impact on climate. Rev Geophys 54(2):278–335. https://doi.org/10.1002/2015rg000511
Kuwata M, Kondo Y, Takegawa N (2009) Critical condensed mass for activation of black carbon as cloud condensation nuclei in Tokyo. J Geophys Res 114:D20202. https://doi.org/10.1029/2009jd012086
Laborde M, Mertes P, Zieger P, Dommen J, Baltensperger U, Gysel M (2012) Sensitivity of the single particle soot photometer to different black carbon types. Atmos Meas Tech 5:1031–1043. https://doi.org/10.5194/amt-5-1031-2012
Laborde M, Crippa M, Tritscher T, Jurányi Z, Decarlo PF, Temime-Roussel B, Marchand N, Eckhardt S, Stohl A, Baltensperger U, Prévôt ASH, Weingartner E, Gysel M (2013) Black carbon physical properties and mixing state in the European megacity Paris. Atmos Chem Phys 13(11):5831–5856. https://doi.org/10.5194/acp-13-5831-2013
Lamb KD, Matsui H, Katich JM, Perring AE, Spackman JR, Weinzierl B, Dollner M, Schwarz JP (2021) Global-scale constraints on light-absorbing anthropogenic iron oxide aerosols. Npj Clim Atmos Sci 4:15. https://doi.org/10.1038/s41612-021-00171-0
Laskin A, Laskin J, Nizkorodov SA (2015) Chemistry of atmospheric brown carbon. Chem Rev 115(10):4335–4382. https://doi.org/10.1021/cr5006167
Lau KM, Kim MK, Kim KM (2006) Asian summer monsoon anomalies induced by aerosol direct forcing: the role of the Tibetan Plateau. Clim Dyn 26:855–864. https://doi.org/10.1007/s00382-006-0114-z
Lighty JS, Veranth JM, Sarofim AF (2000) Combustion aerosols: factors governing their size and composition and implications to human health. J Air Waste Manag Assoc 50(9):1565–1618. https://doi.org/10.1080/10473289.2000.10464197
Liu M, Matsui H (2021) Improved simulations of global black carbon distributions by modifying wet scavenging processes in convective and mixed-phase clouds. J Geophys Res Atmos 126:e2020JD033890. https://doi.org/10.1029/2020jd033890
Liu D, Whitehead J, Alfarra MR, Reyes-Villegas E, Spracklen DV, Reddington CL, Kong S, Williams PI, Ting YC, Haslett S, Taylor JW, Flynn MJ, Morgan WT, McFiggans G, Coe H, Allan JD (2017) Black-carbon absorption enhancement in the atmosphere determined by particle mixing state. Nat Geosci 10:184–188. https://doi.org/10.1038/ngeo2901
Liu D, Taylor JW, Crosier J, Marsden N, Bower KN, Lloyd G, Ryder CL, Brooke JK, Cotton R, Marenco F, Blyth A, Cui Z, Estelles V, Gallagher M, Coe H, Choularton TW (2018) Aircraft and ground measurements of dust aerosols over the west African coast in summer 2015 during ICE-D and AER-D. Atmos Chem Phys 18(5):3817–3838. https://doi.org/10.5194/acp-18-3817-2018
Liu D, He C, Schwarz JP, Wang X (2020a) Lifecycle of light-absorbing carbonaceous aerosols in the atmosphere. Npj Clim Atmos Sci 3:40. https://doi.org/10.1038/s41612-020-00145-8
Liu F, Yon J, Fuentes A, Lobo P, Smallwood GJ, Corbin JC (2020b) Review of recent literature on the light absorption properties of black carbon: refractive index, mass absorption cross section, and absorption function. Aerosol Sci Technol 54(1):33–51. https://doi.org/10.1080/02786826.2019.1676878
Liu M, Matsui H, Hamilton DS, Lamb KD, Rathod SD, Schwarz JP, Mahowald NM (2022) The underappreciated role of anthropogenic sources in atmospheric soluble iron flux to the Southern Ocean. Npj Clim Atmos Sci 5:28. https://doi.org/10.1038/s41612-022-00250-w
Lund MT, Samset BH, Skeie RB, Watson-Parris D, Katich JM, Schwarz JP, Weinzierl B (2018) Short black carbon lifetime inferred from a global set of aircraft observations. Npj Clim Atmos Sci 1:31. https://doi.org/10.1038/s41612-018-0040-x
Matsui H, Kondo Y, Moteki N, Takegawa N, Sahu LK, Koike M, Zhao Y, Fuelberg HE, Sessions WR, Diskin G, Anderson BE, Blake DR, Wisthaler A, Jimenez JL (2011) Accumulation-mode aerosol number concentrations in the Arctic during the ARCTAS aircraft campaign: Long-range transport of polluted and clean air from the Asian continent. J Geophys Res 116:D20217. https://doi.org/10.1029/2011jd016189
Matsui H, Koike M, Kondo Y, Moteki N, Fast JD, Zaveri RA (2013) Development and validation of a black carbon mixing state resolved three-dimensional model: aging processes and radiative impact. J Geophys Res Atmos 118(5):2304–2326. https://doi.org/10.1029/2012jd018446
Matsui H, Mahowald NM, Moteki N, Hamilton DS, Ohata S, Yoshida A, Koike M, Scanza RA, Flanner MG (2018) Anthropogenic combustion iron as a complex climate forcer. Nat Commun 9:1593. https://doi.org/10.1038/s41467-018-03997-0
McConnell JR, Edwards R, Kok GL, Flanner MG, Zender CS, Saltzman ES, Banta JR, Pasteris DR, Carter MM, Kahl JD (2007) 20th-century industrial black carbon emissions altered Arctic climate forcing. Science 317(5843):1381–1384. https://doi.org/10.1126/science.1144856
McMurry PH, Wang X, Park K, Ehara K (2002) The relationship between mass and mobility for atmospheric particles: a new technique for measuring particle density. Aerosol Sci Technol 36(2):227–238. https://doi.org/10.1080/027868202753504083
Michelsen HA, Schulz C, Smallwood GJ, Will S (2015) Laser-induced incandescence: particulate diagnostics for combustion, atmospheric, and industrial applications. Prog Energy Combust Sci 51:2–48. https://doi.org/10.1016/j.pecs.2015.07.001
Mishchenko MI (2014) Electromagnetic scattering by particles and particle groups: an introduction. Cambridge University Press, New York
Miyakawa T, Oshima N, Taketani F, Komazaki Y, Yoshino A, Takami A, Kondo Y, Kanaya Y (2017) Alteration of the size distributions and mixing states of black carbon through transport in the boundary layer in east Asia. Atmos Chem Phys 17(9):5851–5864. https://doi.org/10.5194/acp-17-5851-2017
Moosmüller H, Chakrabarty RK, Arnott WP (2009) Aerosol light absorption and its measurement: a review. J Quant Spectrosc Radiat Transf 110(11):844–878. https://doi.org/10.1016/j.jqsrt.2009.02.035
Mori T, Goto-Azuma K, Kondo Y, Ogawa-Tsukagawa Y, Miura K, Hirabayashi M, Oshima N, Koike M, Kupiainen K, Moteki N, Ohata S, Sinha PR, Sugiura K, Aoki T, Schneebeli M, Steffen K, Sato A, Tsushima A, Makarov V, Omiya S, Sugimoto A, Takano S, Nagatsuka N (2019) Black carbon and inorganic aerosols in arctic snowpack. J Geophys Res Atmos 124(23):13325–13356. https://doi.org/10.1029/2019jd030623
Mori T, Kondo Y, Ohata S, Goto-Azuma K, Fukuda K, Ogawa-Tsukagawa Y, Moteki N, Yoshida A, Koike M, Sinha PR, Oshima N, Matsui H, Tobo Y, Yabuki M, Aas W (2021) Seasonal variation of wet deposition of black carbon at NY-Ålesund, Svalbard. J Geophys Res Atmos 126:e2020JD034110. https://doi.org/10.1029/2020jd034110
Mori T, Kondo Y, Goto-Azuma K, Moteki N, Yoshida A, Fukuda K, Ogawa-Tsukagawa Y, Ohata S, Koike M (2023) Measurement of number and mass size distributions of light-absorbing iron oxide aerosols in liquid water with a modified single-particle soot photometer. Aerosol Sci Technol 57(1):35–49. https://doi.org/10.1080/02786826.2022.2144113
Moteki N (2020) Capabilities and limitations of the single-particle extinction and scattering method for estimating the complex refractive index and size-distribution of spherical and non-spherical submicron particles. J Quant Spectrosc Radiat Transf 243:106811. https://doi.org/10.1016/j.jqsrt.2019.106811
Moteki N (2021) Measuring the complex forward-scattering amplitude of single particles by self-reference interferometry: CAS-v1 protocol. Opt Express 29(13):20688–20714. https://doi.org/10.1364/OE.423175
Moteki N, Kondo Y (2007) Effects of mixing state on black carbon measurements by laser-induced incandescence. Aerosol Sci Technol 41(4):398–417. https://doi.org/10.1080/02786820701199728
Moteki N, Kondo Y (2008) Method to measure time-dependent scattering cross sections of particles evaporating in a laser beam. J Aerosol Sci 39(4):348–364. https://doi.org/10.1016/j.jaerosci.2007.12.002
Moteki N, Kondo Y (2010) Dependence of laser-induced incandescence on physical properties of black carbon aerosols: measurements and theoretical interpretation. Aerosol Sci Technol 44(8):663–675. https://doi.org/10.1080/02786826.2010.484450
Moteki N, Kondo Y, Miyazaki Y, Takegawa N, Komazaki Y, Kurata G, Shirai T, Blake DR, Miyakawa T, Koike M (2007) Evolution of mixing state of black carbon particles: aircraft measurements over the western Pacific in march 2004. Geophys Res Lett 34:L11803. https://doi.org/10.1029/2006gl028943

Moteki N, Kondo Y, Takegawa N, Nakamura S (2009) Directional dependence of thermal emission from nonspherical carbon particles. J Aerosol Sci 40(9):790–801. https://doi.org/10.1016/j.jaerosci.2009.05.003
Moteki N, Kondo Y, Nakayama T, Kita K, Sahu LK, Ishigai T, Kinase T, Matsumi Y (2010a) Radiative transfer modeling of filter-based measurements of light absorption by particles: importance of particle size dependent penetration depth. J Aerosol Sci 41(4):401–412. https://doi.org/10.1016/j.jaerosci.2010.02.002
Moteki N, Kondo Y, Nakamura S (2010b) Method to measure refractive indices of small nonspherical particles: application to black carbon particles. J Aerosol Sci 41(5):513–521. https://doi.org/10.1016/j.jaerosci.2010.02.013
Moteki N, Takegawa N, Koizumi K, Nakamura T, Kondo Y (2011) Multiangle polarimetry of thermal emission and light scattering by individual particles in airflow. Aerosol Sci Technol 45(10):1184–1198. https://doi.org/10.1080/02786826.2011.583299
Moteki N, Kondo Y, Oshima N, Takegawa N, Koike M, Kita K, Matsui H, Kajino M (2012) Size dependence of wet removal of black carbon aerosols during transport from the boundary layer to the free troposphere. Geophys Res Lett 39:L13802. https://doi.org/10.1029/2012gl052034
Moteki N, Kondo Y, Adachi K (2014) Identification by single-particle soot photometer of black carbon particles attached to other particles: laboratory experiments and ground observations in Tokyo. J Geophys Res Atmos 119:1031–1043. https://doi.org/10.1002/2013jd020655
Moteki N, Adachi K, Ohata S, Yoshida A, Harigaya T, Koike M, Kondo Y (2017) Anthropogenic iron oxide aerosols enhance atmospheric heating. Nat Commun 8:15329. https://doi.org/10.1038/ncomms15329
Moteki N, Mori T, Matsui H, Ohata S (2019) Observational constraint of in-cloud supersaturation for simulations of aerosol rainout in atmospheric models. Npj Clim Atmos Sci 2:6. https://doi.org/10.1038/s41612-019-0063-y
Moteki N, Ohata S, Yoshida A, Adachi K (2023) Constraining the complex refractive index of black carbon particles using the complex forward-scattering amplitude. EarthArXiv. https://doi.org/10.31223/X5736W
Murphy DM (2007) The design of single particle laser mass spectrometers. Mass Spectrom Rev 26(2):150–165. https://doi.org/10.1002/mas.20113
Murphy DM, Thomson DS, Mahoney MJ (1998) In situ measurements of organics, meteoritic material, mercury, and other elements in aerosols at 5 to 19 kilometers. Science 282(5394):1664–1669. https://doi.org/10.1126/science.282.5394.1664
Murphy DM, Froyd KD, Bourgeois I, Brock CA, Kupc A, Peischl J, Schill GP, Thompson CR, Williamson CJ, Yu P (2021) Radiative and chemical implications of the size and composition of aerosol particles in the existing or modified global stratosphere. Atmos Chem Phys 21(11):8915–8932. https://doi.org/10.5194/acp-21-8915-2021
Nakayama T, Kondo Y, Moteki N, Sahu LK, Kinase T, Kita K, Matsumi Y (2010) Size-dependent correction factors for absorption measurements using filter-based photometers: PSAP and COSMOS. J Aerosol Sci 41(4):333–343. https://doi.org/10.1016/j.jaerosci.2010.01.004
Ni T, Pinson JA, Gupta S, Santoro RJ (1995) Two-dimensional imaging of soot volume fraction by the use of laser-induced incandescence. Appl Opt 34(30):7083–7091. https://doi.org/10.1364/AO.34.007083
Niemeier U, Timmreck C (2015) What is the limit of climate engineering by stratospheric injection of SO2? Atmos Chem Phys 15(16):9129–9141. https://doi.org/10.5194/acp-15-9129-2015
Ohata S, Schwarz JP, Moteki N, Koike M, Takami A, Kondo Y (2016) Hygroscopicity of materials internally mixed with black carbon measured in Tokyo. J Geophys Res Atmos 121(1):362–381. https://doi.org/10.1002/2015jd024153
Ohata S, Kondo Y, Moteki N, Mori T, Yoshida A, Sinha PR, Koike M (2019) Accuracy of black carbon measurements by a filter-based absorption photometer with a heated inlet. Aerosol Sci Technol 53(9):1079–1091. https://doi.org/10.1080/02786826.2019.1627283
Ohata S, Mori T, Kondo Y, Sharma S, Hyvärinen A, Andrews E, Tunved P, Asmi E, Backman J, Servomaa H, Veber D, Eleftheriadis K, Vratolis S, Krejci R, Zieger P, Koike M, Kanaya Y, Yoshida A, Moteki N, Zhao Y, Tobo Y, Matsushita J, Oshima N (2021a) Estimates of mass absorption cross sections of black carbon for filter-based absorption photometers in the Arctic. Atmos Meas Tech 14(10):6723–6748. https://doi.org/10.5194/amt-14-6723-2021
Ohata S, Koike M, Yoshida A, Moteki N, Adachi K, Oshima N, Matsui H, Eppers O, Bozem H, Zanatta M, Herber AB (2021b) Arctic black carbon during PAMARCMiP 2018 and previous aircraft experiments in spring. Atmos Chem Phys 21(20):15861–15881. https://doi.org/10.5194/acp-21-15861-2021
Ohata S, Yoshida A, Moteki N, Adachi K, Takahashi Y, Kurisu M, Koike M (2018) Abundance of light-absorbing anthropogenic iron oxide aerosols in the urban atmosphere and their emission sources. J Geophys Res Atmos 123(15):8115–8134. https://doi.org/10.1029/2018JD028363
Oshima N, Koike M (2013) Development of a parameterization of black carbon aging for use in general circulation models. Geosci Model Dev 6(2):263–282. https://doi.org/10.5194/gmd-6-263-2013
Oshima N, Koike M, Zhang Y, Kondo Y, Moteki N, Takegawa N, Miyazaki Y (2009) Aging of black carbon in outflow from anthropogenic sources using a mixing state resolved model: Model development and evaluation. J Geophys Res 114:D06210. https://doi.org/10.1029/2008jd010680
Oshima N, Kondo Y, Moteki N, Takegawa N, Koike M, Kita K, Matsui H, Kajino M, Nakamura H, Jung JS, Kim YJ (2012) Wet removal of black carbon in Asian outflow: Aerosol radiative forcing in East Asia (A-FORCE) aircraft campaign. J Geophys Res 117:D03204. https://doi.org/10.1029/2011jd016552
Oshima N, Yukimoto S, Deushi M, Koshiro T, Kawai H, Tanaka TY, Yoshida K (2020) Global and Arctic effective radiative forcing of anthropogenic gases and aerosols in MRI-ESM2.0. Prog Earth Planet Sci 7:38. https://doi.org/10.1186/s40645-020-00348-w
Pendergrass AG, Hartmann DL (2012) Global-mean precipitation and black carbon in AR4 simulations. Geophys Res Lett 39:L01703. https://doi.org/10.1029/2011gl050067
Perring AE, Schwarz JP, Markovic MZ, Fahey DW, Jimenez JL, Campuzano-Jost P, Palm BD, Wisthaler A, Mikoviny T, Diskin G, Sachse G, Ziemba L, Anderson B, Shingler T, Crosbie E, Sorooshian A, Yokelson R, Gao RS (2017) In situ measurements of water uptake by black carbon-containing aerosol in wildfire plumes. J Geophys Res Atmos 122(2):1086–1097. https://doi.org/10.1002/2016jd025688
Petzold A, Ogren JA, Fiebig M, Laj P, Li SM, Baltensperger U, Holzer-Popp T, Kinne S, Pappalardo G, Sugimoto N, Wehrli C, Wiedensohler A, Zhang XY (2013) Recommendations for reporting "black carbon" measurements. Atmos Chem Phys 13:8365–8379. https://doi.org/10.5194/acp-13-8365-2013
Pileci RE, Modini RL, Bertò M, Yuan J, Corbin JC, Marinoni A, Henzing B, Moerman MM, Putaud JP, Spindler G, Wehner B, Müller T, Touch T, Trentini A, Zanatta M, Baltensperger U, Gysel-Beer M (2021) Comparison of co-located refractory black carbon (rBC) and elemental carbon (EC) mass concentration measurements during field campaigns at several European sites. Atmos Meas Tech 14(2):1379–1403. https://doi.org/10.5194/amt-14-1379-2021
Pósfai M, Gelencsér A, Simonics R, Arató K, Li J, Hobbs PV, Buseck PR (2004) Atmospheric tar balls: particles from biomass and biofuel burning. J Geophys Res 109:D06213. https://doi.org/10.1029/2003jd004169
Potenza MAC, Sanvito T, Pullia A (2015) Measuring the complex field scattered by single submicron particles. AIP Adv 5(11):117222. https://doi.org/10.1063/1.4935927
Ramanathan V, Carmichael G (2008) Global and regional climate changes due to black carbon. Nat Geosci 1:221–227. https://doi.org/10.1038/ngeo156
Rathod SD, Hamilton DS, Mahowald NM, Klimont Z, Corbett JJ, Bond TC (2020) A mineralogy-based anthropogenic combustion-iron emission inventory. J Geophys Res Atmos 125(17):e2019JD032114. https://doi.org/10.1029/2019jd032114
Reddington CL, McMeeking G, Mann GW, Coe H, Frontoso MG, Liu D, Flynn M, Spracklen DV, Carslaw KS (2013) The mass and number size distributions of black carbon aerosol over Europe. Atmos Chem Phys 13(9):4917–4939. https://doi.org/10.5194/acp-13-4917-2013
Riemer N, West M, Zaveri R, Easter R (2010) Estimating black carbon aging time-scales with a particle-resolved aerosol model. J Aerosol Sci 41(1):143–158. https://doi.org/10.1016/j.jaerosci.2009.08.009
Romanov AV, Yurkin MA (2021) Single-particle characterization by elastic light scattering. Laser Photon Rev 15(2):2000368. https://doi.org/10.1002/lpor.202000368
Rytov S (1953) The theory of electrical fluctuations and thermal radiation, U.S.S.R. Academy of Science, Moscow. English transl. by U.S. Air Force Cambridge Research Center, Bedford, Massachusetts, Rep. AFCRC–TR–59–162.

Samset BH (2022) Aerosol absorption has an underappreciated role in historical precipitation change. Commun Earth Environ 3:242. https://doi.org/10.1038/s43247-022-00576-6

Samset BH, Stjern CW, Andrews E, Kahn RA, Myhre G, Schulz M, Schuster GL (2018) Aerosol absorption: progress towards global and regional constraints. Curr Clim Change Rep 4(2):65–83. https://doi.org/10.1007/s40641-018-0091-4

Sand M, Samset BH, Myhre G, Gliß J, Bauer SE, Bian H, Chin M, Checa-Garcia R, Ginoux P, Kipling Z, Kirkevåg A, Kokkola H, Le Sager P, Lund MT, Matsui H, van Noije T, Olivié DJL, Remy S, Schulz M, Stier P, Stjern CW, Takemura T, Tsigaridis K, Tsyro SG, Watson-Parris D (2021) Aerosol absorption in global models from AeroCom phase III. Atmos Chem Phys 21(20):15929–15947. https://doi.org/10.5194/acp-21-15929-2021

Schmitt CG, Riggs BL, Horodyskyj UN, Khan AL, Ewing HA, All JD, Sanchez RW (2019) The measurement and impact of light absorbing particles on snow surfaces. Cryosphere Discuss. https://doi.org/10.5194/tc-2019-162

Schulz C, Kock BF, Hofmann M, Michelsen H, Will S, Bougie B, Suntz R, Smallwood G (2006) Laser-induced incandescence: recent trends and current questions. Appl Phys B 83(3):333–354. https://doi.org/10.1007/s00340-006-2260-8

Schulz H, Zanatta M, Bozem H, Leaitch WR, Herber AB, Burkart J, Willis MD, Kunkel D, Hoor PM, Abbatt JPD, Gerdes R (2019) High Arctic aircraft measurements characterising black carbon vertical variability in spring and summer. Atmos Chem Phys 19(4):2361–2384. https://doi.org/10.5194/acp-19-2361-2019

Schuster GL, Dubovik O, Arola A (2016) Remote sensing of soot carbon—part 1: distinguishing different absorbing aerosol species. Atmos Chem Phys 16(3):1565–1585. https://doi.org/10.5194/acp-16-1565-2016

Schuster GL, Andrews E, Chin M, DaSilva A, Johnson B, Moore R, Saito M, Schwarz JP, Stamnes S, van Diedenhoven B, Yang P (2022) The tables of aerosol optics (TAO) project, American Geophysical Union, Fall Meeting 2022. A12M-1272.

Schwarz JP, Gao RS, Fahey DW, Thomson DS, Watts LA, Wilson JC, Reeves JM, Darbeheshti M, Baumgardner DG, Kok GL, Chung SH, Schulz M, Hendricks J, Lauer A, Kärcher B, Slowik JG, Rosenlof KH, Thompson TL, Langford AO, Loewenstein M, Aikin KC (2006) Single-particle measurements of midlatitude black carbon and light-scattering aerosols from the boundary layer to the lower stratosphere. J Geophys Res 111:D16207. https://doi.org/10.1029/2006jd007076

Schwarz JP, Spackman JR, Fahey DW, Gao RS, Lohmann U, Stier P, Watts LA, Thomson DS, Lack DA, Pfister L, Mahoney MJ, Baumgardner D, Wilson JC, Reeves JM (2008a) Coatings and their enhancement of black carbon light absorption in the tropical atmosphere. J Geophys Res 113:D03203. https://doi.org/10.1029/2007jd009042

Schwarz JP, Gao RS, Spackman JR, Watts LA, Thomson DS, Fahey DW, Ryerson TB, Peischl J, Holloway JS, Trainer M, Frost GJ, Baynard T, Lack DA, de Gouw JA, Warneke C, Del Negro LA (2008b) Measurement of the mixing state, mass, and optical size of individual black carbon particles in urban and biomass burning emissions. Geophys Res Lett 35:L13810. https://doi.org/10.1029/2008gl033968

Schwarz JP, Spackman JR, Gao RS, Watts LA, Stier P, Schulz M, Davis SM, Wofsy SC, Fahey DW (2010) Global-scale black carbon profiles observed in the remote atmosphere and compared to models. Geophys Res Lett 37:L18812. https://doi.org/10.1029/2010gl044372

Schwarz JP, Gao RS, Perring AE, Spackman JR, Fahey DW (2013) Black carbon aerosol size in snow. Sci Rep 3:1356. https://doi.org/10.1038/srep01356

Shiraiwa M, Kondo Y, Moteki N, Takegawa N, Miyazaki Y, Blake DR (2007) Evolution of mixing state of black carbon in polluted air from Tokyo. Geophys Res Lett 34:L16803. https://doi.org/10.1029/2007gl029819

Shrivastava M, Cappa CD, Fan J, Goldstein AH, Guenther AB, Jimenez JL, Kuang C, Laskin A, Martin ST, Ng NL, Petaja T, Pierce JN, Thornton JA, Volkamer R, Wang J, Worsnop DR, Zaveri RA, Zelenyuk A, Zhang Q (2017) Recent advances in understanding secondary organic aerosol: implications for global climate forcing. Rev Geophys 55(2):509–559. https://doi.org/10.1002/2016rg000540

Simoneit BR (2000) Biomass burning—a review of organic tracers for smoke from incomplete combustion. Appl Geochem 17(3):129–162. https://doi.org/10.1016/S0883-2927(01)00061-0

Skiles SM, Flanner M, Cook JM, Dumont M, Painter TH (2018) Radiative forcing by light-absorbing particles in snow. Nat Clim Chang 8(11):964–971. https://doi.org/10.1038/s41558-018-0296-5

Slowik JG, Stainken K, Davidovits P, Williams LR, Jayne JT, Kolb CE, Worsnop DR, Rudich Y, DeCarlo PF, Jimenez JL (2004) Particle morphology and density characterization by combined mobility and aerodynamic diameter measurements. Part 2: application to combustion-generated soot aerosols as a function of fuel equivalence ratio. Aerosol Sci Technol 38(12):1206–1222. https://doi.org/10.1080/027868290903916

Slowik JG, Cross ES, Han JH, Davidovits P, Onasch TB, Jayne JT, Williams LR, Canagaratna MR, Worsnop DR, Chakrabarty RK, Moosmüller H, Arnott WP, Schwarz JP, Gao RS, Fahey DW, Kok GL, Petzold A (2007) An intercomparison of instruments measuring black carbon content of soot particles. Aerosol Sci Technol 41(3):295–314. https://doi.org/10.1080/02786820701197078

Snelling DR, Smallwood GJ, Sawchuk RA, Neill WS, Gareau D, Chippior WL, Liu F, Gülder ÖL, Bachalo WD (1999) Particulate matter measurements in a diesel engine exhaust by laser-induced incandescence and the standard gravimetric procedure. SAE Technical Paper No. 1999-01-3653. Doi: https://doi.org/10.4271/1999-01-3653

Spackman JR, Gao RS, Neff WD, Schwarz JP, Watts LA, Fahey DW, Holloway JS, Ryerson TB, Peischl J, Brock CA (2010) Aircraft observations of enhancement and depletion of black carbon mass in the springtime Arctic. Atmos Chem Phys 10(19):9667–9680. https://doi.org/10.5194/acp-10-9667-2010

Stagg BJ, Charalampopoulos TT (1993) Refractive indices of pyrolytic graphite, amorphous carbon, and flame soot in the temperature range 25° to 600°C. Combust Flame 94(4):381–396. https://doi.org/10.1016/0010-2180(93)90121-i

Stephens M, Turner N, Sandberg J (2003) Particle identification by laser-induced incandescence in a solid-state laser cavity. Appl Opt 42(19):3726–3736. https://doi.org/10.1364/ao.42.003726

Stier P, Seinfeld JH, Kinne S, Boucher O (2007) Aerosol absorption and radiative forcing. Atmos Chem Phys 7(19):5237–5261. https://doi.org/10.5194/acp-7-5237-2007

Taylor JW, Allan JD, Allen G, Coe H, Williams PI, Flynn MJ, Le Breton M, Muller JBA, Percival CJ, Oram D, Forster G, Lee JD, Rickard AR, Parrington M, Palmer PI (2014) Size-dependent wet removal of black carbon in Canadian biomass burning plumes. Atmos Chem Phys 14(24):13755–13771. https://doi.org/10.5194/acp-14-13755-2014

Textor C, Schulz M, Guibert S, Kinne S, Balkanski Y, Bauer S, Berntsen T, Berglen T, Boucher O, Chin M, Dentener F, Diehl T, Easter R, Feichter H, Fillmore D, Ghan S, Ginoux P, Gong S, Grini A, Hendricks J, Horowitz L, Huang P, Isaksen I, Iversen I, Kloster S, Koch D, Kirkevåg A, Kristjansson JE, Krol M, Lauer A et al (2006) Analysis and quantification of the diversities of aerosol life cycles within AeroCom. Atmos Chem Phys 6(7):1777–1813. https://doi.org/10.5194/acp-6-1777-2006

Thompson CR, Wofsy SC, Prather MJ, Newman PA, Hanisco TF, Ryerson TB, Fahey DW, Apel EC, Brock CA, Brune WH, Froyd K, Katich JM, Nicely JM, Peischl J, Ray E, Veres PR, Wang S, Allen HM, Asher E, Bian H, Blake D, Bourgeois I, Budney J, Bui PT, Butler A, Campuzano-Jost P, Chang C, Chin M, Commane R, Correa G et al (2022) The NASA atmospheric tomography (ATom) mission: imaging the chemistry of the global atmosphere. Bull Am Meteorol Soc 103(3):E761–E790. https://doi.org/10.1175/bams-d-20-0315.1

Updyke KM, Nguyen TB, Nizkorodov SA (2012) Formation of brown carbon via reactions of ammonia with secondary organic aerosols from biogenic and anthropogenic precursors. Atmos Environ 63:22–31. https://doi.org/10.1016/j.atmosenv.2012.09.012

van de Hulst HC (1957) Light scattering by small particles. John Wiley & Sons Inc, New York

Vander Wal RL, Jensen KA (1998) Laser-induced incandescence: excitation intensity. Appl Opt 37(9):1607–1616. https://doi.org/10.1364/ao.37.001607

Vander Wal RL, Weiland KJ (1994) Laser-induced incandescence: development and characterization towards a measurement of soot-volume fraction. Appl Phys B 59(4):445–452. https://doi.org/10.1007/bf01081067

Vander Wal RL, Ticich TM, Brock Stephens A (1999) Can soot primary particle size be determined using laser-induced incandescence? Combust Flame 116:291–296. https://doi.org/10.1016/s0010-2180(98)00040-6

Vignati E, Karl M, Krol M, Wilson J, Stier P, Cavalli F (2010) Sources of uncertainties in modelling black carbon at the global scale. Atmos Chem Phys 10(6):2595–2611. https://doi.org/10.5194/acp-10-2595-2010

Wang Q, Jacob DJ, Spackman JR, Perring AE, Schwarz JP, Moteki N, Marais EA, Ge C, Wang J, Barrett SR (2014) Global budget and radiative forcing of black carbon aerosol: constraints from pole-to-pole (HIPPO) observations across the Pacific. J Geophys Res Atmos 119(1):195–206. https://doi.org/10.1002/2013jd020824

Wang J, Wang J, Cai R, Liu C, Jiang J, Nie W, Wang J, Moteki N, Zaveri RA, Huang X, Ma N, Chen G, Wang Z, Jin Y, Cai J, Zhang Y, Chi X, Holanda B, Xing J, Liu T, Qi X, Wang Q, Christopher P, Su H, Cheng Y, Wang S, Hao J, Andreae MO, Ding A (2022) Unified theoretical framework for mixing state of black carbon. EarthArXiv. https://doi.org/10.31223/X5C64D

Winstrup M, Vallelonga P, Kjær HA, Fudge TJ, Lee JE, Riis MH, Edwards R, Bertler NAN, Blunier T, Brook EJ, Buizert C, Ciobanu G, Conway H, Dahl-Jensen D, Ellis A, Emanuelsson BD, Hindmarsh RCA, Keller ED, Kurbatov AV, Mayewski PA, Neff PD, Pyne RL, Simonsen MF, Svensson A, Tuohy A, Waddington ED, Wheatley S (2019) A 2700-year annual timescale and accumulation history for an ice core from Roosevelt Island, West Antarctica. Clim past 15(2):751–779. https://doi.org/10.5194/cp-15-751-2019

Yamashita Y, Nakane M, Mori Y, Nishioka J, Ogawa H (2022) Fate of dissolved black carbon in the deep Pacific Ocean. Nat Commun 13:307. https://doi.org/10.1038/s41467-022-27954-0

Yang M, Howell SG, Zhuang J, Huebert BJ (2009) Attribution of aerosol light absorption to black carbon, brown carbon, and dust in China—interpretations of atmospheric measurements during EAST-AIRE. Atmos Chem Phys 9(6):2035–2050. https://doi.org/10.5194/acp-9-2035-2009

Yang Y, Xu X, Zhang Y, Zheng S, Wang L, Liu D, Gustave W, Jiang L, Hua Y, Du S, Tang L (2019) Seasonal size distribution and mixing state of black carbon aerosols in a polluted urban environment of the Yangtze River Delta region, China. Sci Total Environ 654:300–310. https://doi.org/10.1016/j.scitotenv.2018.11.087

Yoshida A, Moteki N, Ohata S, Mori T, Tada R, Dagsson-Waldhauserová P, Kondo Y (2016) Detection of light-absorbing iron oxide particles using a modified single-particle soot photometer. Aerosol Sci Technol 50(3):1–4. https://doi.org/10.1080/02786826.2016.1146402

Yoshida A, Ohata S, Moteki N, Adachi K, Mori T, Koike M, Takami A (2018) Abundance and emission flux of the anthropogenic iron oxide aerosols from the east Asian continental outflow. J Geophys Res Atmos 123(19):11194–11209. https://doi.org/10.1029/2018jd028665

Yoshida A, Moteki N, Ohata S, Mori T, Koike M, Kondo Y, Matsui H, Oshima N, Takami A, Kita K (2020) Abundances and microphysical properties of light-absorbing iron oxide and black carbon aerosols over east Asia and the arctic. J Geophys Res Atmos 125:e2019JD032301. https://doi.org/10.1029/2019jd032301

Yoshida A, Moteki N, Adachi K (2022) Identification and particle sizing of submicron mineral dust by using complex forward-scattering amplitude data. Aerosol Sci Technol 56(7):609–622. https://doi.org/10.1080/02786826.2022.2057839

Yu P, Froyd KD, Portmann RW, Toon OB, Freitas SR, Bardeen CG, Brock C, Fan T, Gao RS, Katich JM, Kupc A, Liu S, Maloney C, Murphy DM, Rosenlof KH, Schill G, Schwarz JP, Williamson C (2019a) Efficient in-cloud removal of aerosols by deep convection. Geophys Res Lett 46(2):1061–1069. https://doi.org/10.1029/2018GL080544

Yu P, Toon OB, Bardeen CG, Zhu Y, Rosenlof KH, Portmann RW, Thornberry TD, Gao RS, Davis SM, Wolf ET, de Gouw J, Peterson DA, Fromm MD, Robock A (2019b) Black carbon lofts wildfire smoke high into the stratosphere to form a persistent plume. Science 365(6453):587–590. https://doi.org/10.1126/science.aax1748

Yu P, Davis SM, Toon OB, Portmann RW, Bardeen CG, Barnes JE, Telg H, Maloney C, Rosenlof KH (2021) Persistent stratospheric warming due to 2019–2020 Australian wildfire smoke. Geophys Res Lett 48:e2021GL092609. https://doi.org/10.1029/2021gl092609

Zaveri RA, Barnard JC, Easter RC, Riemer N, West M (2010) Particle-resolved simulation of aerosol size, composition, mixing state, and the associated optical and cloud condensation nuclei activation properties in an evolving urban plume. J Geophys Res Atmos 115:D17210. https://doi.org/10.1029/2009JD013616

Zhang Y, Kang S, Li C, Gao T, Cong Z, Sprenger M, Liu Y, Li X, Guo J, Sillanpää M, Wang K, Chen J, Li Y, Sun S (2017) Characteristics of black carbon in snow from Laohugou No. 12 glacier on the northern Tibetan Plateau. Sci Total Environ 607–608:1237–1249. https://doi.org/10.1016/j.scitotenv.2017.07.100

Zhao R, Lee AKY, Huang L, Li X, Yang F, Abbatt JPD (2015) Photochemical processing of aqueous atmospheric brown carbon. Atmos Chem Phys 15(11):6087–6100. https://doi.org/10.5194/acp-15-6087-2015

Zheng L, Wu Y (2021) Effects of primary particle size on light absorption enhancement of black carbon aerosols using the superposition T-matrix method. J Quant Spectrosc Radiat Transf 258(1):07388. https://doi.org/10.1016/j.jqsrt.2020.107388

Publisher's Note